Title: Nuclear receptor corepressor 1 controls regulatory T cell subset differentiation and effector function

Authors: Valentina Stolz[1,#], Rafael de Freitas e Silva[1,#], Ramona Rica[1], Ci Zhu[1], Teresa Preglej[1], Patricia Hamminger[1], Daniela Hainberger[1], Marlis Alteneder[1], Lena Müller[1], Monika Waldherr[1], Darina Waltenberger[1], Anastasiya Hladik[2], Benedikt Agerer[3], Michael Schuster[3], Tobias Frey[4], Thomas Krausgruber[3,7], Sylvia Knapp[2], Clarissa Campbell[3], Klaus Schmetterer[4], Michael Trauner[5], Andreas Bergthaler[3,6], Christoph Bock[3,7], Nicole Boucheron[1], Wilfried Ellmeier[1,*]

[1]Medical University of Vienna, Center for Pathophysiology, Infectiology and Immunology, Institute of Immunology, Vienna, Austria.
[2]Medical University of Vienna, Vienna, Department of Medicine I, Laboratory of Infection Biology, Vienna, Austria.
[3]CeMM Research Centre for Molecular Medicine of the Austrian Academy of Sciences, Vienna, Austria.
[4]Medical University of Vienna, Department of Laboratory Medicine, Vienna, Austria.
[5]Medical University of Vienna, Department of Internal Medicine III, Division of Gastroenterology and Hepatology, Hans Popper Laboratory of Molecular Hepatology, Vienna, Austria.
[6]Medical University of Vienna, Vienna, Center for Pathophysiology, Infectiology and Immunology, Institute for Hygiene and Applied Immunology, Austria.
[7]Medical University of Vienna, Center for Medical Statistics, Informatics, and Intelligent Systems, Institute of Artificial Intelligence, Vienna, Austria.

equal first-authorship

***Correspondence:**
Dr. Wilfried Ellmeier
Medical University of Vienna, Center for Pathophysiology, Infectiology and Immunology, Institute of Immunology, Lazarettgasse 19, A-1090 Vienna, Austria.
Email: wilfried.ellmeier@meduniwien.ac.at
Phone: +43 1 40160 33293

Competing interests:
The authors declare no competing interests.

Abstract

FOXP3$^+$ regulatory T cells (Treg cells) are key for immune homeostasis. Here, we reveal that nuclear receptor corepressor 1 (NCOR1) controls naïve and effector Treg cell states. Upon NCOR1 deletion in T cells, effector Treg cell frequencies were elevated in mice and in *in vitro*-generated human Treg cells. NCOR1-deficient Treg cells failed to protect mice from severe weight loss and intestinal inflammation associated with CD4$^+$ T cell transfer colitis, indicating impaired suppressive function. NCOR1 controls transcriptional integrity of Treg cells, since effector gene signatures were already upregulated in naïve NCOR1-deficient Treg cells while effector NCOR1-deficient Treg cells failed to repress genes associated with naïve Treg cells. Moreover, genes related to cholesterol homeostasis including targets of liver X receptor (LXR) were dysregulated in NCOR1-deficient Treg cells. However, genetic ablation of LXRβ in T cells did not revert the effects of NCOR1 deficiency, indicating that NCOR1 controls naïve and effector Treg cell subset composition independent from its ability to repress LXRβ-induced gene expression. Thus, our study reveals that NCOR1 maintains naïve and effector Treg cell states via regulating their transcriptional integrity. We also reveal a critical role for this epigenetic regulator in supporting the suppressive functions of Treg cells *in vivo*.

Introduction

Regulatory T cells (Treg cells) expressing the transcription factor Forkhead box protein P3 (FOXP3) play a crucial role in mediating immune tolerance to self-antigens, regulating the interaction between the host and its commensal flora, and promoting tissue repair. Deficiency or aberrant function of Treg cells triggers autoimmunity and inflammation [1, 2]. Therefore, the development of these cells, as well as their effector functions, must be tightly regulated [3, 4, 5, 6]. The transcription factor FOXP3 is required for the generation, maintenance and suppressive function of Treg cells, and loss of FOXP3 leads to fatal systemic autoimmunity in mice and humans [7, 8, 9]. Upon stimulation, naïve Treg cells (also known as resting Treg cells) undergo differentiation into effector Treg cells (also known as activated Treg cells or effector memory Treg cells) thereby acquiring distinct phenotypes and effector molecules expression [10, 11, 12]. Effector Treg cells exhibit enhanced suppressive function compared to naïve Treg cells and maintain immune tolerance and homeostasis [13, 14]. The conversion of naïve Treg cells into effector Treg cells is accompanied by metabolic reprogramming including relatively higher engagement of aerobic glycolysis over oxidative phosphorylation. This cellular change is necessary to support the function of effector Treg cells and to supply the biosynthetic material needed for their proliferation and expansion [15, 16]. However, the transcriptional pathways involved in effector Treg cell generation remain poorly understood.

The nuclear receptor co-repressor 1 (NCOR1) is a transcriptional regulator that bridges chromatin modifying enzymes and transcription factors [17]. NCOR1 mediates transcriptional repression of nuclear receptors (NRs) such as thyroid hormone (TR), retinoic acid receptors (RAR) and liver X receptor (LXR) in the absence of their ligands via its interaction with members of the HDAC family, in particular HDAC3. NCOR1 is part of larger multi-subunit complexes and also interacts with several other transcription factors unrelated to NRs [17]. We and others have recently identified NCOR1 as an important regulator of T cell development, as T cell-specific deletion of NCOR1 resulted in impaired survival of positively selected NCOR1-null TCRβ^{hi}CD69$^{+/-}$ thymocytes. Furthermore, NCOR1 deficiency also leads to

reduced numbers of peripheral T cells including Treg cells [18, 19]. Leng and colleagues identified a role for NCOR1 in repressing the pro-apoptotic factor BIM in double-positive thymocytes post-signaling, thereby affecting thymocyte survival during positive selection [18]. These data indicate that NCOR1 is essential for positive and negative selection during T cell development, as well as for the generation of the peripheral T cell pool. Additionally, NCOR1 was shown to regulate the transcriptional programs and effector functions of activated Th1 and Th17 cells [20]. However, whether NCOR1 controls the function of immunosuppressive Treg cells has yet to be investigated.

Here, we employed conditional gene targeting approaches to study the role of NCOR1 in Treg cells. NCOR1 was deleted either in all peripheral T cells using *Ncor1*$^{f/f}$ mice crossed with *Cd4*-Cre mice (*Ncor*1$^{f/f}$*Cd4*-Cre, designated as NCOR1-cKO) or selectively in Treg cells using *Ncor1*$^{f/f}$ mice crossed with *Foxp3*-YFP-Cre mice (*Ncor*1$^{f/f}$*Foxp3*-YFP-Cre; designated as NCOR1-cKO^{Foxp3}). Using these mouse models, we analyzed Treg cell generation, Treg cell transcriptomes, and Treg cell function *in vitro* as well as in adoptive transfer colitis. Moreover, we assessed whether NCOR1 is essential for human Treg cell differentiation *in vitro* using CRISPR-Cas9 mediated deletion approaches. Finally, since we observed an upregulation of LXR/RAR activation pathways, we generated NCOR1 and LXRβ double-deficient mice to address whether NCOR1 requires LXRβ to repress effector Treg cell differentiation. With these experimental strategies we identify NCOR1 as a key regulatory molecule controlling naïve and effector Treg cell states in mouse and human by ensuring transcriptional integrity, reveal that NCOR1 restrains effector Treg cell generation independently of LXRβ, and uncover a positive role for NCOR1 in controlling the suppressive function of Treg cells *in vivo*.

Results

Increased frequencies of effector Treg cells in NCOR1-cKO mice

To investigate whether NCOR1 activity is important for FOXP3$^+$ regulatory T cell subset differentiation and function, we characterized Treg cells in *Ncor1*$^{f/f}$ crossed with *Cd4*-Cre mice (designated as NCOR1-cKO). Similar to conventional T cells, Treg cells can be subdivided based on CD44 and CD62L expression into naïve (CD44^{lo}CD62L$^+$) and activated/effector (CD44^{hi}CD62L$^-$) populations [11]. We observed an increase in the proportion of CD44^{hi}CD62L$^-$ effector Treg cells and a corresponding decrease in CD44^{lo}CD62L$^+$ naïve Treg cells in the spleen (Figure 1a and 1b), Lymph node (LN) and mesenteric LN (mLN) (Supplementary Figure 1a and 1b) in the absence of NCOR1. The relative increase in effector Treg cells in NCOR1-cKO mice also correlated with an elevated expression of KLRG1 and CD69 in Treg cells, two markers characteristic of activated/effector Treg cells [21, 22, 23, 24], while the proportion of CD25$^+$ cells within the FOXP3$^+$ Treg cell population was decreased. Moreover, we detected higher percentages of ICOS-expressing Treg cells in NCOR1-cKO mice, and NCOR1-deficient Treg cells expressed elevated levels of GITR in LN and mLN. There was no significant difference in the expression of CTLA4 between WT and NCOR1-cKO Treg cells (Supplementary Figure 1c and 1d). However, total numbers of naïve and effector Treg cells were reduced in NCOR1-cKO mice (Figure 1c). This is due to the overall reduction in Treg cell numbers, caused by the drop in total CD4$^+$ T cells as well as the relative reduction of Treg cells within the CD4$^+$ T cell population in NCOR1-cKO mice, as previously reported [19, 20]. We also tested whether alterations in the proliferation and/or survival of NCOR1-cKO Treg cells contribute to the relative reduction in the frequency of Treg cells within the peripheral CD4$^+$ T cell population. The percentage of Treg cells expressing Ki67, a marker associated with cell proliferation, as well as the expression levels of Ki67 (gMFI) in FOXP3$^+$ cells was similar between splenic WT and NCOR1-cKO Treg cells (Supplementary Figure 2a and 2b). Similarly, there was no difference in cell viability WT and NCOR1-cKO Treg cells (see timepoint 0h; Supplementary Figure 2c). These data suggest that Treg cell proliferation and survival at

steady state are not controlled by NCOR1. Of note, there was no increase in $CD44^{hi}CD62L^{-}$ effector cell subsets within the $FOXP3^{-}$ $CD4^{+}$ T cell population, in fact effector subsets were slightly reduced (Supplementary Figure 2d). Taken together, the flow cytometry analysis indicates that the deletion of NCOR1 in T cells changes the ratio of naïve to effector Treg cells at steady state.

We next investigated whether loss of NCOR1 affects Treg cell differentiation in the thymus per se. Thymic Treg cells commonly develop from CD4SP $CD25^{+}$ progenitor cells which upregulate FOXP3 expression [25, 26], although FOXP3 can also be induced in CD4SP cells before CD25 expression [27]. In the NCOR1-cKO CD4SP population both $CD25^{+}FOXP3^{+}$ and $CD25^{-}FOXP3^{+}$ subsets were reduced in comparison to WT CD4SP cells (Supplementary Figure 2e and 2f). Furthermore, there was an increase in $CD44^{hi}CD62L^{-}$ cells within both the $CD25^{-}$ and $CD25^{+}$ fraction of the $FOXP3^{+}$ CD4SP population in NCOR1-cKO mice (Supplementary Figure 2g). These data indicate that the relative reduction of Treg cells within the $CD4^{+}$ T cell population as well as the change in the relative abundance of naïve and effector Treg cells in NCOR1-cKO mice is (in part) already established during the generation of Treg cells in the thymus.

Increased effector Treg cell subsets upon immunization in NCOR1-cKO mice

Treg cells acquire specialized functions in the periphery. T follicular regulatory (Tfr) cells represent a subset of peripheral effector Treg cells that are induced during an immune response. Tfr cells are defined as $CXCR5^{+}PD1^{+}CD44^{hi}$ $CD4^{+}$ T cells that express FOXP3 [28, 29, 30]. To test whether the generation of Tfr cells is enhanced *in vivo* during an immune response in the absence of NCOR1, WT and NCOR1-cKO mice were immunized subcutaneously (s.c.) with NP-KLH (nitrophenol keyhole limpet hemocyanin) mixed with alum. T cell subsets were analyzed in the draining LNs (dLNs) 6 days later (Figure 1d). Upon immunization, similar percentages of $CXCR5^{+}PD1^{+}CD44^{hi}$ T follicular helper (Tfh) cells were induced within the $CD4^{+}$ T cell population in WT and NCOR1-cKO mice (Figure 1e and 1f). In contrast, the frequency of Tfr cells was higher in NCOR1-cKO mice (Figure 1e and 1f), which

is consistent with our observation that effector Treg cells were increased within the total Treg cell population at steady state. Total numbers of CXCR5^{+}PD1^{+}CD44^{hi} Tfh cells were slightly reduced while the total number of Tfr cells were similar between WT and NCOR1-cKO mice (Figure 1g). Furthermore, we detected decreased expression of CD25 in CXCR5^{+}PD1^{+}CD44^{hi}FOXP3^{+} Tfr cells isolated from NCOR1-cKO mice compared to WT mice (Figure 1h and 1i), in line with the observation that the most mature Tfr cells in the germinal center downregulate CD25 [31]. Together, this data suggests that NCOR1 restrains the generation of activated/effector Treg cells not only at steady state but also upon immunization.

To study whether NCOR1 controls the generation of activated Treg cells by modulating events induced by TCR stimulation, we next analyzed proximal TCR signaling pathways in *ex vivo* isolated WT and NCOR1-cKO Treg cells. We assessed the expression of phospho-ERK$^{T202/Y204}$, phospho-AKT^{S473} and phospho-S6$^{S240/244}$ in FOXP3^{+} Treg cells cultured in the presence of anti-CD3/anti-CD28 for 10 minutes, 2 hours and 24 hours (Supplementary Figure 2h). Despite a trend for higher levels of phospho-ERK$^{T202/Y204}$, phospho-AKT^{S473} and phospho-S6$^{S240/244}$ in NCOR1-cKO Treg cells at several early time points, we only observed a significant difference for phospho-AKT^{S473} at the 2 hours timepoint, which might indicate altered mTORC2 activation [32, 33]. Next, we assessed whether reduced viability upon activation could contribute to the altered effector Treg cell population in NCOR1-cKO by culturing splenocytes in the presence of anti-CD3/anti-CD28 for up to 72 hours. While there was no significant difference in the viability of WT and NCOR1-cKO Treg cells after 4 or 24 hours of activation, we observed a decrease in the percentage of viable NCOR1-cKO Treg cells after 72 hours (Supplementary Figure 2c). Overall, these data suggest that NCOR1-cKO Treg cells might display a slightly higher transient degree of activation after TCR triggering but their viability decline a few days later.

NCOR1 controls effector phenotypes in murine and human iTreg cells

To test whether NCOR1 deletion affects the differentiation or effector features of *in vitro* generated Treg cells (iTreg cells), we activated and cultured naïve CD4^{+} T cells isolated from

WT and NCOR1-cKO mice for three days in the presence of IL-2 and TGFβ. There was no difference in FOXP3 expression between WT and NCOR1-deficient iTreg cells (Figure 2a). However, NCOR1-cKO iTreg cells exhibited reduced viability compared to WT iTreg cells, and CFSE-labeling experiments showed a trend towards their reduced proliferation (Figure 2a). In contrast, CD44 and ICOS were upregulated in iTreg cells lacking NCOR1 compared to WT iTreg cells (Figure 2b), suggesting enhanced effector features in NCOR1-deficient iTreg cells.

iTreg cells are known to downregulate FOXP3 upon restimulation with anti-CD3/anti-CD28 in the absence of TGFβ [34]. To test whether NCOR1 is important for the maintenance of FOXP3 expression, we restimulated WT and NCOR1-cKO iTreg cells under these conditions for 4 days. There was no difference in the expression of FOXP3 between WT and NCOR1-cKO Treg cells, indicating that NCOR1 function is dispensable for the maintenance of FOXP3 expression in iTreg cells (Figure 2c).

To investigate whether loss of NCOR1 changes the distribution of naïve and effector populations in human Treg cells, we deleted NCOR1 in human $CD4^+$ T cells cultured in Treg-inducing conditions using CRISPR-Cas9 mediated knockout approaches. Loss of NCOR1 led to an increase in the fraction of human $CD4^+$ T cells expressing high levels of FOXP3 (Figure 2d). We also analyzed the expression of CD45RA and CD45RO to distinguish naïve ($CD45RA^+CD45RO^-$) from effector/memory ($CD45RA^-CD45RO^+$) T cells [35, 36]. There was a slight reduction of NCOR1-deficient human $CD4^+$ T cells cultured in Treg cell-inducing conditions with a $CD45RA^+CD45RO^-$ naïve expression phenotype (Figure 2e and 2f), although no change was detected in the frequency of $CD45RA^-CD45RO^+$ effector Treg cells after NCOR1 deletion. Moreover, CD27, a marker associated with a naive phenotype in $CD4^+$ T cells [37], was downregulated in NCOR1 knockout human $CD4^+$ T cells (Figure 2e and 2f). Together these data indicate a cross-species conservation of NCOR1 function in regulating effector Treg cell differentiation in mouse and human $CD4^+$ T cells. Furthermore, the data indicate that deletion of NCOR1 in human $CD4^+$ T cells facilitates the generation of $FOXP3^+$ T cells.

NCOR1 regulates naïve and effector Treg cell states in a Treg cell-intrinsic manner

To study whether the alterations in naïve and effector Treg cell subset composition is due to a Treg cell-intrinsic requirement for NCOR1, we generated mixed bone marrow chimeric mice. For this, we transferred a 1:1 mix of either WT (CD45.1$^+$) and *NCOR1*$^{f/f}$ (WT; CD45.2$^+$) or WT (CD45.1$^+$) and NCOR1-cKO (NCOR1-cKO; CD45.2$^+$) bone marrow cells into lethally irradiated *Rag2*$^{-/-}$ mice and analyzed recipient mice 6 weeks after reconstitution (Figure 3a). Within the spleen of mixed BM chimeric mice, we detected reduced percentages of Treg cells within the CD4$^+$CD45.2$^+$ cell population (Figure 3b and 3c) of NCOR1-cKO CD45.2$^+$ cells relative to WT. Within the CD45.2$^+$ FOXP3$^+$ Treg cell population, the CD44^{hi}CD62L$^-$ effector Treg cell subset was increased in the absence of NCOR1 compared to the WT CD45.2$^+$ Treg cell population (Figure 3b and 3d). In contrast, there were similar percentages of CD44^{hi}CD62L$^-$ cells in FOXP3$^+$CD45.1$^+$ CD4$^+$ T cells in WT:WT and WT:NCOR1-cKO BM chimeric mice (Figure 3e and 3f). To further exclude the possibility of Treg cell-extrinsic effects upon *Ncor1* deletion in *Cd4*-Cre mice, we took advantage of the Treg cell-specific *Foxp3*-YFP-Cre deleter strain [38] to delete *Ncor1* (*Ncor1*$^{f/f}$ *Foxp3*-YFP-Cre mice, designated as NCOR1-cKO^{Foxp3}). Indeed, we observed Treg cell-specific deletion of the *Ncor1* alleles in *Ncor1*$^{f/f}$ YFP$^+$ (i.e., FOXP3$^+$) cells isolated from NCOR1-cKO^{Foxp3} mice (Supplementary Figure 3a), although we cannot formally exclude a stochastic activation of *Foxp3*-Cre in non-Treg cells in some mice as previously reported for other targeted gene loci [39]. In line with the results from NCOR1-cKO mice, Treg cell-specific deletion of *Ncor1* resulted in a relative increase in splenic CD44^{hi}CD62L$^-$ effector Treg cells compared to WT^{Foxp3} (*Ncor1*$^{+/+}$ *Foxp3*-YFP-Cre) mice (Supplementary Figure 3b and 3c), while the total cell numbers of CD44^{hi}CD62L$^-$ effector Treg cells were slightly but not significantly increased (Supplementary Figure 3d). In contrast to *Ncor1* deletion in *Cd4*-Cre mice, deletion of *Ncor1* in *Foxp3*-Cre mice did not alter the frequencies or total numbers of CD4$^+$FOXP3$^+$ cells (Supplementary Figure 3e and 3f). Together, these data indicate that the increase of effector Treg cell subsets in NCOR1-cKO mice is Treg cell-intrinsic. Moreover, these data also show that NCOR1 controls naïve and effector Treg cell subset composition in cells already expressing the lineage-defining transcription factor FOXP3.

NCOR1 is essential for Treg cell-mediated protection against intestinal inflammation

Next, we analyzed the impact of NCOR1 deletion on Treg cell effector function. We first investigated whether NCOR1 controls the expression of the anti-inflammatory cytokine TGFβ. *Ex vivo* PMA/ionomycin stimulation revealed an increase in TGFβ expression in NCOR1-cKO Treg cells compared to WT Treg cells (Supplementary Figure 4a and 4b). To assess whether NCOR1-cKO Treg cells display an altered suppressive activity on a per cell basis, we performed *in vitro* suppression assays in which increasing numbers of Treg cells are tested for their ability to restrain the proliferation of WT $CD4^+$ T cells activated by dendritic cells (DC, Supplementary Figure 4c and 4d). To facilitate Treg cell isolation, we crossed WT and NCOR1-cKO mice to the DEREG *Foxp3*-eGFP reporter strain, in which GFP expression is driven by *Foxp3* regulatory elements [40]. There was no difference in the suppressive activity of splenic NCOR1-cKO.DEREG $FOXP3^+$ Treg cells compared to WT.DEREG Treg cells.

To assess whether the proportional increase in effector Treg cells correlated with an enhanced suppressive function *in vivo*, we employed a naïve $CD4^+$ T cell adoptive transfer colitis model, in which $CD4^+$ T cell-mediated disease in recipient *Rag2*-deficient mice is accompanied by several pathological changes including body weight reduction, infiltration of immune cells and loss of colonic crypt structure [41]. Co-transfer of Treg cells suppresses T cell-mediated autoimmune diseases and prevents immune pathology [42]. Therefore, naive WT $CD4^+FOXP3^-$ T cells ($CD45.1^+$) were transferred into *Rag2*$^{-/-}$ mice together with Treg cells that were isolated from either WT.DEREG or NCOR1-cKO.DEREG mice ($CD45.2^+$) and recipient mice were monitored over a period of 8 weeks (Figure 4a). Mice that co-received NCOR1-cKO Treg cells lost significantly more weight compared to mice co-receiving WT Treg cells, and the weight loss upon transfer of NCOR1-deficient Treg cells was similar to mice that received naïve $CD4^+$ T cells only (Figure 4b). Although colon length was not significantly different in any of the groups analyzed (Figure 4c), the increased weight loss of mice co-transferred with NCOR1-cKO Treg cells also correlated with a more severe colonic inflammation compared to mice co-transferred with WT Treg cells, indicated by a disruption of

crypt structures and enhanced T cell infiltration (Figure 4d). Together, these data indicate that NCOR1 is required for Treg cell function *in vivo.*

To understand the cellular basis of why NCOR1-deficient Treg cells failed to protect against colitis, we characterized lymphocyte subsets in recipient *Rag2*$^{-/-}$ mice including small intestinal intraepithelial lymphocytes (SI-IEL), lamina propria cells (SI-LP) as well as lymphocytes from spleen and mLNs. The frequencies of NCOR1-deficient FOXP3^{+} Treg cells trended towards a reduction within the SI-IEL and SI-LP cell populations, although total Treg numbers were comparable in mice receiving WT or NCOR1-cKO Treg cells (Figure 5a and 5b). NCOR1-cKO Treg cell (CD45.2^{+}) frequencies were significantly reduced in spleen and mLNs (Figure 5b) accompanied with slightly increased frequencies of effector CD4^{+} T cells (CD45.1^{+}) in the spleen and mLNs of mice that received NCOR1-deficient Treg cells compared to mice that received WT Treg cells (CD45.2^{+}) (Figure 5c). However, we detected no differences in the numbers of effector CD4^{+} T cells (CD45.1^{+}) (Figure 5c), or in the percentages of IL-17A^{+}, IFNγ^{+} and IL-17A^{+}IFNγ^{+} expressing CD4^{+} T cells in recipient mice that either received WT or NCOR1-deficient Treg cells (Supplementary Figure 5a and 5b). Although we cannot formally rule out that lower numbers of NCOR1-cKO Treg cells in the spleen and mLNs may contribute to disease development, these results suggest that colitis may arise from a local functional impairment of NCOR1-deficient Treg cells at earlier time points following T cell transfer.

NCOR1 ensures transcriptional integrity of naïve and effector Treg cells

As demonstrated above, NCOR1 deletion led to Treg cell-intrinsic alterations that changed the relative abundance of naïve to effector Treg cells. To reveal the underlying NCOR1-dependent transcriptional changes, we performed low-input RNA sequencing (RNA-seq) [43]. To exclude differences in transcriptomes due to the different naïve and effector Treg ratios in WT and NCOR1-cKO, we sorted the same number of naïve (CD44^{lo}CD62L^{+}) and effector (CD44^{hi}CD62L^{-}) Treg cell subsets from the corresponding DEREG mice and sequenced them separately (Figure 6a). We detected a total of 1567 genes being differentially expressed (FDR

≤ 0.05) in NCOR1-deficient naive Treg cells compared to WT naïve Treg cells, with 540 genes up- and 1027 genes downregulated in the absence of NCOR1 (Figure 6b and Supplementary Table 1). RNA-seq of effector Treg cell subsets revealed that 574 genes were differentially expressed (FDR ≤ 0.05) between NCOR1-deficient and WT effector Treg cells. Of these genes, 299 were upregulated and 275 were downregulated in the absence of NCOR1 (Figure 6b and Supplementary Table 2). To identify transcriptional changes related to well-defined biological states or processes that are altered in the absence of NCOR1, a Gene Set Enrichment Analysis (GSEA) [44] using the hallmark gene sets of the Molecular Signatures Database (MSigDB) was performed. This uncovered several gene sets that were either enriched or underrepresented in the absence of NCOR1 (a list of all identified hallmark gene sets from this analysis for naïve and effector cells can be found in Supplementary Table 3 and Supplementary Table 4, respectively). Among the altered signatures we identified an enrichment of “MYC target genes v.2” gene sets, MTORC1 signaling”, “Estrogen response”, “E2F targets” and “cholesterol homeostasis” in NCOR1-cKO naïve Treg cells compared to their WT counterparts (Figure 6c) and these gene sets were also enriched in effector NCOR1-cKO Treg cells (Figure 6c). Among the hallmark gene sets that were underrepresented in the absence of NCOR1 was “IL2_Stat5_signaling” (Figure 6c). To further assess transcriptional changes in the absence of NCOR1, a pathway analysis was performed [45]. This also indicated a strong upregulation of pathways and genes associated with cholesterol biosynthesis in both naïve and effector NCOR1-cKO Treg cell subsets (Supplementary Figure 6a and 6b, Supplementary Table 5 and Supplementary Table 6), similar to observations previously made in conventional naïve NCOR1-cKO $CD4^+$ T cells [20]. Of note, the upregulation of the “Cholesterol homeostasis” hallmark gene set in NCOR1-deficient naive Treg cells (Figure 6c) did not lead to accumulation of membrane cholesterol as revealed by comparable Filipin III staining intensities between NCOR1-cKO $CD4^+CD25^+$ Treg cells and WT Treg cells (Supplementary Figure 6c). However, the ATP-binding cassette transporters *Abca1* and *Abcg1*, important regulators of cholesterol efflux [46], were upregulated in naïve (*Abca1*) and effector (*Abca1, Abcg1*) NCOR1-cKO Treg cells (Supplementary Figure 6d). Thus, we

conclude that despite an elevated cholesterol biosynthesis pathway in NCOR1-cKO Treg cells, there is no accumulation of membrane-inserted cholesterol, likely due to enhanced cholesterol export caused by increased expression of *Abca1* and *Abcg1*.

Since the proportion of effector Treg cells is increased in NCOR1-cKO mice, we next addressed the question whether NCOR1 deficiency in naïve Treg cells results in the induction of transcriptional signatures characteristic of effector Treg cell subsets. Therefore, we defined an "effector Treg gene set" based on our RNA-seq data that contained the top 100 genes upregulated (based on FC differences, FDR ≤ 0.05) in effector WT Treg cells compared to naïve WT Treg cells (see Supplementary Table 7 for the list of genes). GSEA with this pre-defined gene list revealed enrichment of the "effector Treg gene set" in naïve NCOR1-cKO Treg cells compared to naïve WT Treg cells (Figure 6d). This indicates that *Ncor1* deletion leads to an upregulation of an effector gene signature in naïve NCOR1-cKO Treg cells per se. Moreover, GSEA also revealed an enrichment of a "naïve Treg gene set" (i.e. the top 100 genes upregulated in WT naïve Treg cells compared to WT effector Treg cells) in effector NCOR1-cKO Treg cells (Figure 6e). Taken together, our RNA-seq analysis indicates that naïve $CD44^{lo}CD62L^{+}$ Treg cells lacking NCOR1 inherently display an effector Treg signature and vice-versa. Thus, NCOR1 is essential for establishing and/or maintaining transcriptional programs that define and potentially regulate naïve and effector Treg cell states.

NCOR1 regulates naïve and effector Treg cell states in a LXRß independent manner

The nuclear receptor liver X receptor (LXR) acts as a cholesterol sensor and is a crucial regulator of cholesterol biosynthesis [47]. Two isoforms of LXR, namely LXRα (encoded by the *Nr1h3* gene) and LXRβ (encoded by *Nr1h2*) are known [48, 49]. Naïve and effector WT Treg cells expressed high levels of *Nr1h2* but virtually no *Nr1h3,* and this isoform-specific expression pattern was maintained in NCOR1-cKO Treg cells compared to WT Treg cells (Supplementary Figure 7a). In the absence of LXR ligands, NCOR1 interacts with LXR and inhibits the expression of LXR target genes [50, 51]. Upon ligand binding, NCOR1 dissociates from LXR leading to its activation and the expression of target genes [52]. Due to the observed

upregulation of hallmark gene sets “Cholesterol homeostasis” (Figure 6c) and LXR/RXR activation pathways (Supplementary Figure 6a) in NCOR1-cKO Treg cells, we investigated whether a disrupted LXRβ-NCOR1 interaction in Treg cells results in enhanced effector Treg differentiation using two experimental strategies based on pharmacological and genetic approaches. First, to test whether LXR activation contributed to effector Treg cell development, we differentiated naïve WT $CD4^+$ T cells into *in vitro* induced Treg cells (iTreg cells) in the presence of the LXR agonist GW3965 [53]. GW3965 treatment did not alter the percentage of $FOXP3^+$ cells, however resulted in a small but significant increase in the fraction of $CD44^{hi}$ cells (Supplementary Figure 7b). GW3965 treatment mildly affected cell viability and proliferation at low concentrations (up to 4μM), but showed more severe effects at a higher concentration (8μM) (Supplementary Figure 7b). Next, to dissect a potential functional interaction between NCOR1 and LXRβ in the induction of effector Treg cells *in vivo*, we employed a genetic approach and intercrossed NCOR1-cKO mice with LXRβ-cKO ($Nr1h2^{f/f}$) mice [54] to generate NCOR1-LXRβ-cDKO double-deficient mice. To obtain a sufficiently high number of mice for the analysis, we established independent breeding colonies for NCOR1-cKO.LXRβ-cKO as well as for NCOR1-LXRβ-cDKO mice and used the corresponding *Cre*-negative littermates as WT controls (i.e., $Ncor1^{f/f}$, designated as WT^{Ncor1}; $Nr1h2^{f/f}$, as WT^{Lxrb}; and $Ncor1^{f/f}$,$Nr1h2^{f/f}$ as $WT^{Ncor1/Lxrb}$, respectively). In agreement with a previous study [55], we observed a strong reduction in the frequencies of splenic T cells in the absence of LXRβ (Supplementary Figure 8a and 8b). Within the $TCR\beta^+$ population, $CD4^+$ T cells were slightly reduced, while the frequency of $CD8^+$ T cells was not altered (Supplementary Figure 8b and 8c). Of note, NCOR1-LXRβ-cDKO mice also exhibited a severe reduction of T cell numbers and slightly lower frequencies of $CD4^+$ T cells as observed in LXRβ-cKO mice (Supplementary Figure 8a-c). Interestingly, the Treg cell frequency within the LXRβ-cKO $CD4^+$ T cell population in the spleen was higher compared to WT littermate controls (Figure 7a and 7b), in contrast to NCOR1-cKO mice where a 2-fold relative decrease was observed (Figure 7a and 7b). NCOR1-LXRβ-cDKO mice also exhibited a higher representation of Treg cells amongst the $CD4^+$ T cell population (Figure 7a and 7b), suggesting that loss of LXRβ is sufficient to rescue

the low Treg cell frequency phenotype seen in NCOR1-cKO mice. Within the LXRβ-cKO Treg cell population, there was a tendency of a mild increase in $CD44^{hi}CD62L^{-}$ effector cell frequencies (P=0.058), while $CD44^{lo}CD62L^{+}$ naïve Treg cells were not changed (Figure 7c and 7d). This suggests that LXRβ deletion using CD4-*Cre* only had a small effect on the differentiation of naïve to effector Treg cells. In contrast, splenocytes from NCOR1-LXRβ-cDKO mice displayed a strong increase in the frequency of $CD44^{hi}CD62L^{-}$ effector Treg cells along with a severe decrease in naïve Treg cells (Figure 7c and 7d), similar to NCOR1-cKO mice. This indicates that loss of LXRβ did not revert alterations in the ratio of naïve to effector Treg cells induced by NCOR1 deletion. On the contrary, within the Treg cell population of some splenocytes from NCOR1-LXRβ-cDKO mice more than 50% of effector Treg cells were detected (Figure 7c and 7d), a frequency not reached in NCOR1-cKO mice (Figure 1b and 7d). This might suggest a minor contribution of LXRβ in the generation of effector Treg cells in the absence of NCOR1.

The transcription factor MYC plays a key role in the transition to an effector Treg cell state, as well as in the metabolic programming of effector Treg cells [56, 57]. NCOR1 also has been shown to cooperate with c-MYC [58]. We observed an induction of Myc target genes (V1 and V2 gene sets) in the absence of NCOR1 (Figure 6c) and our RNA-seq data revealed that *Myc* expression was upregulated both in naïve and in effector NCOR1-cKO Treg cells in comparison to the corresponding WT subsets (Figure 6b, Supplementary Table 3 and Supplementary Table 4). Therefore, in a next step we investigated whether MYC protein expression levels were affected by the absence of NCOR1, LXRβ or both. Intracellular staining revealed no difference in MYC protein levels between WT^{Ncor1} and NCOR1-cKO naïve Treg cells and slightly lower MYC levels in effector Treg cells (Supplementary Figure 9a), contrasting with the observed upregulation of *Myc* mRNA levels and MYC target genes. MYC protein expression was significantly increased in naïve $CD44^{lo}CD62L^{+}$ LXRβ-cKO and NCOR1-LXRβ-cDKO $FOXP3^{+}$ Treg cells in comparison to the respective WT^{Lxrb} and $WT^{Ncor1/Lxrb}$ controls (Supplementary Figure 9a), suggesting that loss of LXRβ has a dominant effect on MYC levels in this Treg cell subset. However, elevated MYC protein levels in LXRß-

deficient Treg cells were not sufficient to induce an increase in effector Treg cells. This suggests that NCOR1 might restrain MYC activity, which in turn might contribute to the observed increase in effector Treg cells upon NCOR1 deletion. Of note, while LXRβ-cKO mice also displayed higher MYC protein levels in effector Treg cells relative to their WT counterparts, this was reverted in NCOR1-LXRβ-cDKO animals (Supplementary Figure 9a). We also assessed how CRISPR-Cas9 mediated-deletion of NCOR1 affected MYC expression levels in human $CD4^+$ T cells cultured in Treg cell-inducing conditions (Figure 2d). Loss of NCOR1 led to an increase in the fraction of human $CD4^+$ T cells expressing high levels of MYC (Supplementary Figure 9b and 9c). The MYC^{hi} population of human $CD4^+$ T cells contained a higher percentage of FOXP3-expressing cells in the absence of NCOR1 when compared to $CD4^+$ T cells treated with non-targeting (NT)-sgRNAs (Supplementary Figure 9b and 9c). Similar to murine Treg cells, MYC protein levels were similar between NCOR1-deficient and WT human $FOXP3^+$ $CD4^+$ T cells.

Taken together, these data indicate that NCOR1 controls naïve and effector Treg cell states, and the relative distribution of Treg cell subsets in an LXRβ-independent manner. Moreover, our data also suggest that NCOR1 restrains MYC activity, which might contribute to the observed increase in effector Treg cells upon NCOR1 deletion.

Discussion

In this study we demonstrate that the transcriptional regulator NCOR1 is a key factor controlling naïve and effector Treg cell subset distribution at steady state and during immune responses in a Treg cell-intrinsic manner. We, and others, have previously reported that loss of NCOR1 in T cells using *Cd4*-Cre results in developmental alterations during positive/negative selection, as well as in reduced survival of single-positive cells [18, 19]. The Treg-specific deletion of *Ncor1* using the *Foxp3*-Cre deleter strain resulted in an increase in effector Treg cells as observed in mice with a pan T cell-specific deletion using *Cd4*-Cre. However, in contrast to *Ncor1*$^{f/f}$ *Cd4*-Cre mice [19], there was no overall decrease in the percentage of the FOXP3^{+} T cell population in NCOR1-cKO^{Foxp3} mice compared to WT^{Foxp3} mice at steady state. This suggests that Treg cell survival is not dependent on NCOR1 once Treg cell lineage differentiation has been initiated. These data therefore rule out the possibility that changes in the frequencies of naïve and effector subsets within the Treg cell population are due to positive/negative selection defects or due to the reduced survival of single-positive cells in NCOR1-cKO mice [18, 19]. Therefore, our data indicate that NCOR1 controls the establishment of Treg cell subset homeostasis once *Foxp3* expression, and thus Treg cell lineage differentiation, has been induced.

Effector Treg cell subsets have a higher suppressive activity and are crucial for maintaining immune homeostasis in peripheral tissues [13]. Therefore, one might have expected that the increase in effector Treg cells results in an enhanced suppressive function of the NCOR1-deficient Treg cell population. Interestingly, there was no difference in the suppressive activity between WT and NCOR1-cKO Treg cells *in vitro*. In addition, in an adoptive CD4^{+} T cell transfer colitis model, even co-transferred NCOR1-cKO Treg cells failed to protect recipient mice from weight loss and intestinal tissue damage in comparison to co-transferred WT Treg cells. We observed an overall decrease of NCOR1-deficient Treg cells in recipient mice, although the extent of the reduction varied among various lymphoid tissues. This might suggest either that NCOR1 is part of a regulatory network that integrates lymphoid

tissue-specific signals for tissue-specific Treg cell maintenance, or that NCOR1 controls the ability of Treg cells to home to different tissues, at least in an adoptive transfer setting. We detected a strong decrease in NCOR1-cKO Treg cells in mLNs after transfer. Since it has been shown that Treg cells home to mLNs early after transfer and proliferate there until colon inflammation is resolved [59], one might speculate that the failure to prevent colitis is caused by the reduction in Treg numbers in gut-draining LNs. However, intestinal Treg cell numbers were not altered within the SI-IEL population and SI-LP cells, suggesting that the disease was aggravated (at least in part) due to an impaired suppressive function of Treg cells in the absence of NCOR1. Further evidence that effector Treg cells might not be fully functional comes from our RNA-seq analysis. Our GSEA data indicated an upregulation of an "effector Treg gene set" in naïve Treg cells, thus potentially a "priming" of naïve NCOR1-deficient Treg cells towards the acquisition of an effector phenotype. However, a "naive Treg gene set" was enriched in NCOR1-deficient effector Treg cells. Thus, NCOR1-cKO Treg cells that upregulated CD44 ($CD44^{hi}$) and downregulated CD62L ($CD62L^{-}$), and hence are classified as effector Treg cells, still have transcriptional features of naïve Treg cells in comparison to WT effector Treg cells. Consequently, NCOR1-cKO $CD44^{hi}CD62L^{-}$ Treg cells might not represent fully functional effector Treg cells. This suggests that NCOR1 is essential in establishing naïve and effector Treg cell states.

Another important finding of our study is that NCOR1 controls naïve and effector Treg states in a LXRβ-independent manner. LXRβ is a key transcription factor of the nuclear receptor family regulating the expression of genes required for cholesterol and lipid metabolism. In the absence of activating ligands, LXRβ target genes are repressed due to the interaction of LXRβ with NCOR1 and associated repressor complexes that contain chromatin modifying molecules such as HDAC3 [47, 50, 51]. LXRβ regulates T cell proliferation and function and is crucial for maintaining cholesterol homeostasis in T cells [60]. The observed upregulation of several pathways associated with cholesterol biosynthesis in NCOR1-deficient Treg cells pointed to an activation of LXRβ-mediated transcriptional circuits and hence to the induction of (some) LXRβ target genes. This might be linked to the enhanced effector Treg

differentiation, substantiated by the observation that LXR agonist GW3965 treatment of WT iTreg cells phenocopied the increased expression of CD44 as observed in NCOR1-cKO Treg cells and in human $CD4^+$ T cells with an NCOR1 knockdown. However, our genetic data demonstrated that deletion of LXRβ in the T cell lineage did not recapitulate the increase in $CD44^{hi}$ $CD62L^-$ effector Treg cells in the spleen observed in NCOR1-cKO mice. The combined deletion of NCOR1 and LXRβ resulted in a strong increase in LXRβ-NCOR1 effector Treg cells and a corresponding severe reduction in naïve Treg cells, similar to the phenotype observed in NCOR1-cKO mice. This strongly suggests that NCOR1 controls the relative composition of naïve and effector Treg cell subsets in a LXRß-independent manner. On the other hand, some LXRβ-NCOR1 mice displayed more than 50% of $CD44^{hi}CD62L^-$ effector cells among the Treg cell population, which was not observed in NCOR1-cKO mice. This suggests that LXRβ might have a minor role in these processes, at least in the absence of NCOR1. Of note, and as previously reported [55], LXRβ deficiency resulted in a relative increase in $FOXP3^+$ T cells among the $CD4^+$ T cell population, while $FOXP3^+$ T cells within the $CD4^+$ T cell lineage was reduced in the absence of NCOR1. LXRβ deletion on top of NCOR1 deletion reverted the relative decrease in Treg cells, which suggests that NCOR1 controls the generation of Treg cells in an LXRβ-dependent manner. NCOR1 suppresses LXRβ or counteracts LXRβ-induced pathways, which itself restrains the generation of $FOXP3^+$ Treg cells. Loss of NCOR1 potentially enhances LXRβ activity or LXRβ-induced pathways, thereby reducing Treg cell frequency. In contrast, deletion of LXRβ (in the presence or absence of NCOR1) abolishes the restraining activity of LXRβ-induced pathways, resulting in increased frequencies of Treg cells among the $CD4^+$ T cell population (Supplementary Figure 10). Our RNA-seq also revealed an upregulation of MYC target genes in NCOR1-cKO Treg cells which correlated with increased *Myc* gene expression, and we even observed an upregulation of MYC protein expression by flow cytometry in LXRβ and NCOR1/LXRβ-deficient T cells. MYC is an essential driver for the differentiation of naive Treg cells into effector cells [56]. However, elevated MYC protein levels in LXRß-deficient Treg cells were not sufficient to induce an increase in effector Treg cells. This suggests that NCOR1 might restrain MYC activity and that

a dysregulated MYC activity might be one of the contributing factors leading to a relative increase in effector Treg cells in the absence of NCOR1.

It must be acknowledged that our study has some limitations. Further investigations are needed to understand to which extent NCOR1 controls effector Treg differentiation in an LXRβ-independent and LXRβ-dependent manner. It has also been reported that LXRβ-deficient Treg cells, in a bone marrow chimeric setting, exhibit decreased expression of CD44 and increased expression of CD62L [54]. However, this decrease in effector Treg cells (based on CD44 and CD62L expression) might be an indirect effect, since LXRβ also controls fitness and functionality of activated Treg cells [54]. Additional studies are warranted to determine how NCOR1 and LXRβ containing complexes control Treg homeostasis and effector Treg differentiation. These might include experiments to determine NCOR1 and LXRβ target binding sites in order to elucidate which target genes are (co-)regulated by NCOR1 and LXRβ during FOPX3$^+$ Treg cell differentiation, and whether T cell activation disrupts NCOR1 and LXRβ interaction. Moreover, it has not been addressed whether NCOR1 modulates the activity of other nuclear receptors and transcription factors in Treg cells or how this might contribute to naïve and effector Treg cell states. In addition, NCOR1 controls Th1 and Th17 cells [20], however it remains to be determined whether NCOR1 is essential for maintaining T cell function in general or whether Th cell subset specific functions exist.

In summary, here we report that NCOR1 is a key member of the transcriptional network that controls FOXP3$^+$ regulatory T cell subset differentiation and function. NCOR1 antagonizes LXRß-induced pathways that restrain the generation of FOXP3$^+$ Treg cells, while NCOR1 controls naïve and effector Treg cell subset distribution independently of LXRß. Moreover, NCOR1 is essential for the proper suppressive function Treg cells. We propose that NCOR1 is essential for maintaining naïve and effector Treg cell states by ensuring the integrity of naïve and effector transcriptional programs in FOXP3$^+$ Treg cells, as well as linking their proper differentiation with their functionality.

Materials and Methods

Animal models

Animal experiments were evaluated by the ethics committees of the Medical University of Vienna and approved by the Austrian Federal Ministry for Education, Science and Research (GZ:BMBWF-66.009/0039-V/3b/2019, GZ:BMBWF-66.009/0326-V/3b/2019). Animals were maintained in research facilities of the Department for Biomedical Research at the Medical University of Vienna. Animal husbandry and experiments were performed under national laws in agreement with guidelines of the Federation of European Laboratory Animal Science Associations (FELASA), which correspond to Animal Research: Reporting of *in vivo* Experiments from the National Center for the Replacement, Refinement and Reduction of Animals in Research (ARRIVE) guidelines. *Ncor1*$^{f/f}$ mice were kindly provided by Johan Auwerx. *Cd4*-Cre mice were kindly provided by Chris Wilson. *Foxp3*-Cre mice were kindly provided by Alexander Rudensky. DEREG mice were kindly provided by Tim Sparwasser. CD45.1^{+} and *Rag2*$^{-/-}$ mice were kindly provided by Jochen Hühn. Mice analyzed were 8–12 weeks of age and of mixed sex, except *Foxp3*-Cre mice of which only males were analyzed.

Genotyping of mice

The PCR for the *Ncor1* deletion (floxed band: 346bp. delta band: 246bp) was carried out for 5 min at 96°C, followed by 39 cycles of 30 s at 94°C, 30 s at 56°C, and 1 min at 72°C. The PCR for the *Cd4*-Cre transgene (300bp) was carried out for 5 min at 96°C, followed by 39 cycles of 30 s at 94°C, 30 s at 56°C, and 1 min at 72°C. The PCR for the DEREG (GFP) transgene (450 bp) was carried out for 1 min at 96°C, followed by 35 cycles of 1 min at 94°C, 1 min at 60°C, and 1 min at 72°C. The PCR for the *Foxp3*-Cre transgene (346 bp) was carried out for 1 min at 94°C, followed by 34 cycles of 30 s at 94°C, 30 s at 60°C, and 45 s at 72°C. Primer: *Ncor1* floxed and deletion (#31): 5'-TTGGCCTTGGAGTAAATGCTGTGAG -3'. *Ncor1* floxed and deletion (#32): 5'-GGAAACTACCTACCTGAATCCATGG-3'. *Ncor1* deletion (#29):

5′- GAA CTA AGG ACA GGA AGG TAC AGG G-3’. *Cd4*-Cre forward: 5’-TCT CTG TGG CTG GCA GTT TCT CCA-3’. *Cd4*-Cre reverse: 5’-TCA AGG CCA GAC TAG GCT GCC TAT-3’. DEREG forward: GCG AGG GCG ATG CCA CCT ACG GCA-3’. DEREG reverse: 5’-GGG TGT TCT GCT GGT AGT GGT CGG-3’. *Foxp3*-Cre forward: 5’-AGG ATG TGA GGG ACT ACC TCC TGT A-3’. *Foxp3*-Cre reverse: 5’-TCC TTC ACT CTG ATT CTG GCA ATT T-3’. *Nr1h2(Lxrb)* floxed forward: 5’ – ACT AAC CCC ACA TTA CCG TGA GGC – 3’. *Nr1h2(Lxrb)* floxed reverse: 5’ – AGG TGC CAG GGT TCT TGC AGT – 3’.

Purification of CD4$^+$ T Cells

Cells from spleen, axillary, brachial, and inguinal lymph nodes (LN) were isolated, pooled and single cell suspensions were made using a 70µm cell strainer (Corning) in a 6-well plate (Sarstedt) containing PBS (Sigma) with 2% fetal bovine serum (FCS) (Biowest). Red blood cells were removed using BD Pharm Lyse (BD Biosciences). Cells were resuspended in PBS/FCS containing a mastermix of biotinylated antibodies (Gr-1, B220, NK1.1, CD11b, CD11c, CD8α, TER-119, CD44 and CD25). CD4$^+$ T cells were enriched by negative depletion using magnetic streptavidin beads (MagniSort SAV Negative Selection beads; Invitrogen) according to the manufacturer’s instructions. Biotinylated antibodies against Ly-6G/Ly-6C (clone: RB6-8C5), CD45R/B220 (clone: RA3-6B2), NK1.1 (clone: PK136), CD11c (clone: N418), CD11b (clone: MEL1/70), CD8α (clone: 53–6.7), TER-119 (clone: TER-119), CD44 (clone: IM7) and CD25 (clone: PC61) were purchased from Biolegend. For some experiments, cells were further sorted into naïve CD4$^+$ T cells (CD25$^-$CD44^{lo}CD62L$^+$) on a SH800 cell sorter (SONY).

Flow Cytometric analysis

Ex vivo isolated T cells and *in vitro*-cultured T cells were incubated with Fc-block (1:250; BD Biosciences) followed by surface staining. Dead cells were excluded using Fixable Viability Dye eFluor 506 or 780 (Thermo Fisher Scientific) according to the manufacturer’s protocol.

For intracellular transcription factor and cytokine staining, cells were fixed and permeabilized using the Foxp3 Staining Buffer Set (Thermo Fisher Scientific) according to the manufacturer's protocol and stained with the appropriate antibodies. Cells were additionally stained with CellTrace Violet Proliferation dye (Thermo Fisher Scientific) wherever indicated. Flow cytometry data was acquired using a BD FACS Fortessa flow cytometer (BD Biosciences) and analyzed using FlowJo v10.2 software (TreeStar). Gating strategies are shown in Supplementary Figure 11.

Flow cytometry antibodies

The following anti-mouse antibodies were used for flow cytometry: CD19 (clone: 6D5, Biolegend), CD25 (clone: PC61, BD Biosciences), CD4 (clone: RM4-5, Biolegend), CD44 (clone: IM7, Biolegend), CD45.1 (clone: A20, Biolegend), CD45.2 (clone: 104, Biolegend), CD62L (clone: MEL-14, Biolegend), CD69 (clone: H1.2F3, Thermo Fisher Scientific), CD8 (clone: 53-6.7, BD Biosciences), CD11c (clone: E418, eBioscience), CTLA4 (clone: UC10-4B9, Biolegend), CXCR5 (clone: L138D7, Biolegend), FOXP3 (clone: FJK-16s, Thermo Fisher Scientific), GITR (clone: REA980, Miltenyi Biotec), ICOS (clone: 7E.17G9, Thermo Fisher Scientific), IFNγ (clone: XMG1.2, Biolegend), IL-17A (clone: TC11-18H10.1, Biolegend), KI67 (clone: 16A8, Biolegend), KLRG1 (clone: 2F1, Biolegend), MYC (clone: Y69, Abcam), PD1 (clone: 29F.1A12, Biolegend), p-AKT (clone: D9E, Cell Signalling), p-ERK (clone: 20A, BD Phosflow), p-S6 (clone: D68F8, Cell Signalling), TCRβ (clone: H57-597, Thermo Fisher Scientific), TGFβ (clone: EPR21143, Abcam), CD80 (clone: 16-10A1, Biolegend), CD86 (clone: GL1, Biolegend), MHCII (clone: M5/114.15.2, eBioscience). The following anti-human antibodies were used for flow cytometry: CD45RA (clone: HI100, Biolegend), CD45RO (clone: UCHL1, Biolegend), CD25 (clone: BC96, Biolegend), CD27 (clone: O323, Biolegend). FOXP3 (clone: PCH101, eBioscience), MYC (clone: Y69, Abcam).

***In vitro* suppression assays**

The experiment was performed as described previously [61]. In brief, FACS-purified CD45.1$^+$ CD4$^+$CD44^{lo}CD62L^{hi} cells were labeled with 20 μM cell proliferation dye eFluor450 (eBioscience) for 10 min at 37°C before culture and activated in the presence of 1 × 10^5 antigen-presenting cells (irradiated CD45.2$^+$ splenocytes) and 1 μg/ml anti-CD3ε (BD Biosciences). 5 × 10^4 responder T cells were cultured in U-bottom 96-well plates in T cell medium (supplemented with 1 mM sodium pyruvate and 100 mM non-essential amino acids) at different ratios with FACS-purified CD45.2$^+$ eGFP$^+$ Treg cells isolated from the spleen and LNs of WT.DEREG and NCOR1-cKO.DEREG mice. After 72 hours, cells were harvested and stained with appropriate antibodies and subjected to flow cytometric analysis.

Adoptive Transfer Colitis

4 x 10^5 flow cytometry-sorted naive (CD25$^-$CD44^{lo}CD62L$^+$) CD4$^+$ T cells from CD45.1$^+$ congenic mice were injected *i.p.* into *Rag2*$^{-/-}$ mice together with either 1 x 10^5 CD45.2$^+$ flow cytometry-sorted WT.DEREG or NCOR1-cKO.DEREG Treg cells only. Control *Rag2*$^{-/-}$ mice did not receive any cells. Weight of the mice was monitored over a course of 8 weeks and mice were subsequently sacrificed for organ analysis. T cells were isolated from spleen and mLNs as described above, stained with appropriate antibodies and subjected to flow cytometric analysis. For SI-LP and SI-IEL isolation, small intestines (SIs) were isolated and stool and mucus were removed. The tissue was transferred into petri dishes, cut into small pieces and washed 3 times by addition of 40ml wash solution (1 X HBSS, HEPES-bicarbonate (pH 7.2) and 2% FBS) and vortexing for 15 seconds. The samples were filtered through 100 μm cell strainers and subsequently incubated in 20 ml EDTA solution (10% FBS, 1 X HBSS, 15 mM HEPES, 1 mM EDTA, pH 7.2) at 37°C whilst shaking at 200rpm. Subsequently, remaining tissue was digested in 30ml Collagenase solution (RPMI 1640 supplemented with 1mM MgCl2, 1mM CaCl2, 5% FBS, and 100 units/ml collagenase D (Gibco, Thermo Fisher Scientific) for 1 hour, followed by a Percoll (Sigma) gradient centrifugation at 2000rpm for 30 minutes at room temperature. Cells from the gradient were collected, washed and resuspended in PBS supplemented with 2% FCS. Cells were further stained with Fixable

Viability Dye eFluor 506 (Thermo Fisher Scientific) and appropriate antibodies and subjected to flow cytometric analysis. For intracellular cytokine detection cells were stimulated with 25 ng/ml PMA and 750 ng/ml ionomycin (both Sigma-Aldrich) in the presence of GolgiStop (BD Biociences). For histological analysis, swiss rolls [62] were prepared from colons of diseased mice as previously described [61].

Histology Microscopy

Fixed tissue samples were processed with a tissue processor (Thermo Fisher Scientific). For hematoxylin and eosin (H&E) stainings, histologic evaluation was performed on 5µm thick sections and stained with hematoxylin and eosin. High power field images (i.e. 400x magnification) were collected from each colon tissue. At least 4 loci were examined from each slide to ensure unbiased analysis.

Generation of Bone Marrow Chimeric mice

Mixed bone marrow chimeric mice were generated as previously described [63]. After six weeks, reconstituted mice were sacrificed and organs were collected as described above. Cells were further stained with Fixable Viability Dye eFluor 506 (Thermo Fisher Scientific) and appropriate antibodies and subjected to flow cytometric analysis.

Immunization studies

WT and NCOR1-cKO mice were injected via the footpad with 10µg NP-KLH (Keyhole Limpet Hemocyanin) (Biosearch Technologies) together with 10µl Imject™ Alum Adjuvant (Thermo Fisher Scientific). 6 days later, the popliteal (draining) lymph node was isolated and single cell suspension was prepared as described above. Cells were further stained with Fixable Viability Dye eFluor 506 (Thermo Fisher Scientific) and appropriate antibodies and subjected to flow cytometric analysis.

Low input RNA Sequencing of *ex vivo* isolated Treg cells

$CD4^+$ T cells were isolated from spleen and lymph nodes as described above and between 5 x 10^4 and 5 x 10^5 $CD4^+eGFP^+CD44^{hi}CD62L^-$ (effector Treg) and $CD4^+eGFP^+CD44^{lo}CD62L^+$ (naïve Treg) cells from either WT.DEREG or NCOR1-cKO.DEREG mice were FACS purified. Total RNA was prepared from cell lysates using the RNeasy Mini Kit (Qiagen) and RNase-Free DNase Set (Qiagen) according to manufacturer's protocol. Three biological replicates were generated for each genotype and Treg subset. Each biological replicate was prepared with pooled cells isolated from three individual mice. RNA and library concentrations were determined using Qbit 2.0 Fluorometric Quantitation (Life Technologies). RNA and library integrities were determined using Experion Automated Electrophoresis System (Bio-Rad). Library preparation and RNA Sequencing were performed by the Biomedical Sequencing facility at CeMM (Research Center for Molecular Medicine of the Austrian Academy of Sciences, Vienna, Austria) using low-input Smart-seq2 [43]. The libraries were sequenced using the Illumina HiSeq 3000 platform and the 50-bp single-read configuration.

Bioinformatic analysis of RNA Sequencing data

Raw sequencing data were processed with Illumina2 bam-tools 1.17 to generate sample-specific, unaligned BAM files. Sequence reads were mapped onto the mouse genome assembly build mm10 (a flavor of GRCm38) using TopHat 2.0.13 [56]. Gene expression values (reads per kilobase exon per million mapped reads) were calculated with Cufflinks 2.2.1 [57]. Volcano plots were generated using the R package EnhancedVolcano (1.22.0). Downstream pathway analysis was performed using the gene set enrichment analysis (GSEA) tools provided by the Broad Institute [36] or ingenuity pathway analysis (IPA) (QIAGEN Inc.) [58] using default settings. GSEA for hallmark signatures of the MSigDb was performed in R (version 4.3.1) employing the packages msigdbr (7.5.1), fgsea (1.26.0), dplyr (1.1.2), ggplot2(3.4.2), tibble(3.2.1), genekitr(1.2.5), forcats (1.0.0) and org.Mm.eg.db (3.17.0). Differential expression modelling was done with the Bioconductor (3.12) package DESeq2 (1.30.0), running under R 4.0.0.

iTreg differentiation culture

Enriched naïve $CD4^+$ T cells were isolated from WT.DEREG and NCOR1-cKO.DEREG mice (8-12 weeks) as described above and cultured in a 48-well plate (500.000 cells/well) (Sarstedt) in T cell medium supplemented with 2ng/ml TGFβ (R&D) and 100 U/ml rhIL-2 (PeproTech) in the presence of plate bound anti-CD3ε (1 µg/mL) (BD Biosciences) and anti-CD28 (3 µg/mL) (BD Biosciences). After 72h, cells were harvested and stained with Fixable Viability Dye eFluor 506 (Thermo Fisher Scientific) and appropriate antibodies and subjected to flow cytometric analysis.

Treg cell viability assay

Isolated WT and NCOR1-cKO splenocytes were cultured in the presence of anti-CD3/anti-CD28 for 72 hours. Cell viability (using Fixable Viability Dye eFluor 780 (Thermo Fisher Scientific) was assessed at 0 hours (i.e. *ex vivo*), 4 hours or 24 hours of activation

Pharmacological activation of liver X receptor (LXR) using GW3965

iTreg cultures were performed as described and simultaneously treated with different concentrations of GW3965 (Sigma) diluted in DMSO (Sigma), as indicated. After 72h, cells were harvested and stained with Fixable Viability Dye eFluor 506 (Thermo Fisher Scientific) and appropriate antibodies and subjected to flow cytometric analysis.

Filipin III staining

Ex vivo isolated splenocytes were stained with anti-CD4 and anti-CD25 antibodies for 30 minutes in PBS supplemented with 2% FCS. After washing, cells were fixed with 2% formaldehyde in PBS for 1 hour at room temperature. After fixation, cells were washed three times and formaldehyde carryover was quenched using 1.5mg/ ml Glycine in PBS for 10 minutes at room temperature. After washing, cells were stained with Filipin III solution (50µg/ml) (Sigma) in PBS and incubated for 2 hours at room temperature. After staining, cells were washed three times and subjected to flow cytometric analysis.

CRISPR-Cas9 mediated deletion of NCOR1

All functional assays were performed in IMDM (Gibco, Thermo Fisher Scientific) supplemented with 10% of fetal calf serum (Gibco) and 10 µg/mL of gentamicin (Gibco). Peripheral blood draws were performed from healthy human volunteers in accordance with the Ethics Committee of the Medical University of Vienna (EC number EK 1150/2015). Mononuclear cells were isolated by standard Ficoll-Paque centrifugation. Naive human $CD4^+$ T cells were isolated using the EasySep Human Naïve CD4 T Cell Iso Kit II (Stem Cell Technologies) according to the manufacturers' instructions. Purity of isolated cells was assessed by flow cytometry and found >95% for all specimens. Subsequently, CRISPR-Cas9 knockout of human NCOR1 was performed as described previously [64]. In detail, 1µL of a mixture of three NCOR1 specific crRNAs (Alt-R® CRISPR-Cas9 crRNA; total concentration 320µM; sequences:GGAATCGAAGCGACCACGTCTGG,TAACCAGCCATCAGATACCAAGG,CGGTGTTTCTGCTCCACAGGAGG; underlined is the PAM sequence) were mixed with 1µL tracr RNA (320µM; all Integrated DNA Technologies, Newark, NJ, USA) and hybridized for 10 min at room temperature. The crRNA-tracr RNA duplex was subsequently complexed with 0.7µL recombinant Cas9 (Alt-R® S.p. Cas9 Nuclease V; 10µg/µL; IDT) for 30min at 37°C. Similarly, a control RNP complex was assembled using a non-targeting crRNA (Alt-R® CRISPR-Cas9 Negative Control crRNA #1; IDT). For electroporation, 1 x 10^6 purified naive T cells were resuspended in 15µL buffer P3 + 5µL Supplement 1 (P3 Primary Cell 4D-NucleofectorTM X Kit S; Lonza) and mixed with 2.7µL RNP in the 16-well strips provided in the kit. Cells were electroporated on a 4D nucleofector (4D-Nucleofector Core Unit, 4D-Nucleofector X Unit; Lonza) using the pulse code EH100. Immediately afterwards, 80µl pre-warmed fresh medium was added to the cells. After a one hour resting period cells were transferred to 24-well plates and incubated for three days in medium containing 10U/mL recombinant human IL-2 (Peprotech) to allow establishment of the knockout. CRISPR-Cas9 knockout efficiency was determined by Sanger sequencing of the target sites of the three gRNAs and analyzed using

the Synthego inference of CRISPR edits analysis tool (ICE v2 CRISPR Analysis Tool; Synthego, Menlo Park, CA). The knockout score defining frameshift insertions/deletions was found to be >65% for at least two of the three loci in all samples tested.

For polarization of induced regulatory T cells (iTreg), cells were preincubated for 1 hour with 100 U/mL IL-2 (Peprotech) + 100 nM all trans retinoic acid (atRA, Sigma Aldrich) + 5 ng/mL TGFβ (PeproTech), stimulated with anti-CD3/anti-CD28 coated dynabeads (Thermo Fisher Scientific) (beads:cell ratio 1:2) and cultured for 7 days as described previously [65]. After polarization, *in vitro* cultured cells were washed and resuspended in PBS supplemented with 2% FCS. Cells were further stained with appropriate antibodies and subjected to flow cytometric analysis. Intracellular staining for transcription factors was performed using the Foxp3 Staining Buffer Set (Thermo Fisher Scientific) according to the manufacturer's protocol.

Statistical analysis

No statistical methods were used to predetermine the sample size. All statistical analyses were performed using Prism 8 Software (GraphPad Inc). As indicated in each figure legend, p-values were calculated using either unpaired two-tailed Student's t-test, one-way or two-way ANOVA followed by Tukey's multiple comparison test or a t-test and Wilcoxon-ranked column statistics. No data were excluded and no specific randomization of animals or blinding of investigators was applied.

Data availability

All data supporting the findings of this study are available within the article and its supplementary information files. RNA Sequencing data have been deposited in the GEO database under the accession number GSE185984. Source data are available upon request from the authors.

Author Contributions

V.S. helped with study design, performed the majority of the experiments, analyzed and interpreted the data, and co-wrote the manuscript. R.S. generated and analyzed LXRß-cKO and NCOR1/LXRß-cDKO mice, interpreted data and co-wrote parts of the manuscript. R.R, C.Z., T.P., P.H., D.H., M.A., L.M., D.W., A.H., B.A. and N.B. assisted with additional experiments. K.S. and T.F. performed CRISPR-Cas9 mediated deletion of NCOR1. C.C: provided *Nr1h2(Lxrb)*$^{f/f}$ mice. M.S. and T.K. helped with preparation of RNA sequencing data and analysis. S.K., M.T., A.B. and C.B. provided critical input for the manuscript. W.E. designed and funded the project, interpreted the data, supervised the project, and co-wrote the manuscript. All authors reviewed the manuscript.

Acknowledgements

We thank Johan Auwerx for providing floxed-*Ncor1* mutant mice. W.E., C.B., and N.B. were supported by the Austrian Science Fund (FWF) Special Research Program F70. W.E. was supported by FWF projects P19930, P23641, P26193, P29790, P35372; and by the FWF and Medical University of Vienna doctoral programs (DK W1212) “Inflammation and Immunity” and (DOC 32 doc.fund) “TissueHome”. V.S. was supported by the FWF and Medical University of Vienna doctoral programs (DK W1212) “Inflammation and Immunity”. P.H. was supported by a DOC fellowship of the Austrian Academy of Sciences. D.H. received a L’Oréal Austria Fellowship supported by the Austrian Commission for UNESCO in cooperation with the Austrian Academy of Sciences. M.T. was supported by the FWF and Medical University of Vienna doctoral programs (DK W1212) “Inflammation and Immunity”. A.B. was supported by the FWF and Medical University of Vienna doctoral programs (DK W1212) “Inflammation and Immunity”. K.S. was supported by the FWF project P34728. N.B. was supported by the FWF project P30885. S.K. received support via the FWF Special Research Programs F54 and F61. We thank Lois Cavanagh for English language editing.

References

1. Sakaguchi, S. *et al.* Regulatory T Cells and Human Disease. *Annu Rev Immunol* **38**, 541-566 (2020).
2. Sumida, T.S., Cheru, N.T. & Hafler, D.A. The regulation and differentiation of regulatory T cells and their dysfunction in autoimmune diseases. *Nat Rev Immunol* **24**, 503-517 (2024).
3. Josefowicz, S.Z., Lu, L.F. & Rudensky, A.Y. Regulatory T cells: mechanisms of differentiation and function. *Annu Rev Immunol* **30**, 531-564 (2012).
4. Li, X. & Zheng, Y. Regulatory T cell identity: formation and maintenance. *Trends Immunol* **36**, 344-353 (2015).
5. Kitagawa, Y. & Sakaguchi, S. Molecular control of regulatory T cell development and function. *Curr Opin Immunol* **49**, 64-70 (2017).
6. Savage, P.A., Klawon, D.E.J. & Miller, C.H. Regulatory T Cell Development. *Annu Rev Immunol* **38**, 421-453 (2020).
7. Hori, S., Nomura, T. & Sakaguchi, S. Control of regulatory T cell development by the transcription factor Foxp3. *Science* **299**, 1057-1061 (2003).
8. Fontenot, J.D., Gavin, M.A. & Rudensky, A.Y. Foxp3 programs the development and function of CD4+CD25+ regulatory T cells. *Nat Immunol* **4**, 330-336 (2003).
9. Khattri, R., Cox, T., Yasayko, S.A. & Ramsdell, F. An essential role for Scurfin in CD4+CD25+ T regulatory cells. *Nat Immunol* **4**, 337-342 (2003).
10. Cretney, E., Kallies, A. & Nutt, S.L. Differentiation and function of Foxp3(+) effector regulatory T cells. *Trends Immunol* **34**, 74-80 (2013).
11. Levine, A.G., Arvey, A., Jin, W. & Rudensky, A.Y. Continuous requirement for the TCR in regulatory T cell function. *Nat Immunol* **15**, 1070-1078 (2014).
12. Contreras-Castillo, E., Garcia-Rasilla, V.Y., Garcia-Patino, M.G. & Licona-Limon, P. Stability and plasticity of regulatory T cells in health and disease. *J Leukoc Biol* **116**, 33-53 (2024).

13. Liston, A. & Gray, D.H. Homeostatic control of regulatory T cell diversity. *Nat Rev Immunol* **14**, 154-165 (2014).

14. Buszko, M. & Shevach, E.M. Control of regulatory T cell homeostasis. *Curr Opin Immunol* **67**, 18-26 (2020).

15. Shi, H. & Chi, H. Metabolic Control of Treg Cell Stability, Plasticity, and Tissue-Specific Heterogeneity. *Front Immunol* **10**, 2716 (2019).

16. Carbone, F. *et al.* Metabolic Plasticity of Regulatory T Cells in Health and Autoimmunity. *J Immunol* **212**, 1859-1866 (2024).

17. Horlein, A.J. *et al.* Ligand-independent repression by the thyroid hormone receptor mediated by a nuclear receptor co-repressor. *Nature* **377**, 397-404 (1995).

18. Wang, J. *et al.* NCoR1 restrains thymic negative selection by repressing Bim expression to spare thymocytes undergoing positive selection. *Nat Commun* **8**, 959 (2017).

19. Muller, L. *et al.* The corepressor NCOR1 regulates the survival of single-positive thymocytes. *Scientific reports* **7**, 15928 (2017).

20. Hainberger, D. *et al.* NCOR1 Orchestrates Transcriptional Landscapes and Effector Functions of CD4(+) T Cells. *Front Immunol* **11**, 579 (2020).

21. Yu, L. *et al.* CD69 enhances immunosuppressive function of regulatory T-cells and attenuates colitis by prompting IL-10 production. *Cell Death Dis* **9**, 905 (2018).

22. Dias, S. *et al.* Effector Regulatory T Cell Differentiation and Immune Homeostasis Depend on the Transcription Factor Myb. *Immunity* **46**, 78-91 (2017).

23. Cortés, J.R. *et al.* Maintenance of immune tolerance by Foxp3+ regulatory T cells requires CD69 expression. *J Autoimmun* **55**, 51-62 (2014).

24. Cheng, G. *et al.* IL-2 receptor signaling is essential for the development of Klrg1+ terminally differentiated T regulatory cells. *J Immunol* **189**, 1780-1791 (2012).

25. Lio, C.W. & Hsieh, C.S. A two-step process for thymic regulatory T cell development. *Immunity* **28**, 100-111 (2008).

26. Burchill, M.A. *et al.* Linked T cell receptor and cytokine signaling govern the development of the regulatory T cell repertoire. *Immunity* **28**, 112-121 (2008).

27. Tai, X. *et al.* Foxp3 transcription factor is proapoptotic and lethal to developing regulatory T cells unless counterbalanced by cytokine survival signals. *Immunity* **38**, 1116-1128 (2013).

28. Wollenberg, I. *et al.* Regulation of the germinal center reaction by Foxp3+ follicular regulatory T cells. *J Immunol* **187**, 4553-4560 (2011).

29. Linterman, M.A. *et al.* Foxp3+ follicular regulatory T cells control the germinal center response. *Nat Med* **17**, 975-982 (2011).

30. Chung, Y. *et al.* Follicular regulatory T cells expressing Foxp3 and Bcl-6 suppress germinal center reactions. *Nat Med* **17**, 983-988 (2011).

31. Wing, J.B. *et al.* A distinct subpopulation of CD25(-) T-follicular regulatory cells localizes in the germinal centers. *Proc Natl Acad Sci U S A* **114**, E6400-e6409 (2017).

32. Sarbassov, D.D., Guertin, D.A., Ali, S.M. & Sabatini, D.M. Phosphorylation and regulation of Akt/PKB by the rictor-mTOR complex. *Science* **307**, 1098-1101 (2005).

33. Szwed, A., Kim, E. & Jacinto, E. Regulation and metabolic functions of mTORC1 and mTORC2. *Physiol Rev* **101**, 1371-1426 (2021).

34. Floess, S. *et al.* Epigenetic control of the foxp3 locus in regulatory T cells. *PLoS Biol* **5**, e38 (2007).

35. Terry, L.A., Brown, M.H. & Beverley, P.C. The monoclonal antibody, UCHL1, recognizes a 180,000 MW component of the human leucocyte-common antigen, CD45. *Immunology* **64**, 331-336 (1988).

36. Sanders, M.E. *et al.* Human memory T lymphocytes express increased levels of three cell adhesion molecules (LFA-3, CD2, and LFA-1) and three other molecules (UCHL1, CDw29, and Pgp-1) and have enhanced IFN-gamma production. *J Immunol* **140**, 1401-1407 (1988).

37. De Jong, R. *et al.* The CD27- subset of peripheral blood memory CD4+ lymphocytes contains functionally differentiated T lymphocytes that develop by persistent antigenic stimulation in vivo. *Eur J Immunol* **22**, 993-999 (1992).

38. Rubtsov, Y.P. *et al.* Regulatory T cell-derived interleukin-10 limits inflammation at environmental interfaces. *Immunity* **28**, 546-558 (2008).

39. Franckaert, D. *et al.* Promiscuous Foxp3-cre activity reveals a differential requirement for CD28 in Foxp3^{+} and Foxp3^{-} T cells. *Immunol Cell Biol* **93**, 417-423 (2015).

40. Lahl, K. *et al.* Selective depletion of Foxp3+ regulatory T cells induces a scurfy-like disease. *J Exp Med* **204**, 57-63 (2007).

41. Kiesler, P., Fuss, I.J. & Strober, W. Experimental Models of Inflammatory Bowel Diseases. *Cell Mol Gastroenterol Hepatol* **1**, 154-170 (2015).

42. Powrie, F., Leach, M.W., Mauze, S., Caddle, L.B. & Coffman, R.L. Phenotypically distinct subsets of CD4+ T cells induce or protect from chronic intestinal inflammation in C. B-17 scid mice. *Int Immunol* **5**, 1461-1471 (1993).

43. Picelli, S. *et al.* Full-length RNA-seq from single cells using Smart-seq2. *Nat Protoc* **9**, 171-181 (2014).

44. Subramanian, A. *et al.* Gene set enrichment analysis: a knowledge-based approach for interpreting genome-wide expression profiles. *Proc Natl Acad Sci U S A* **102**, 15545-15550 (2005).

45. Krämer, A., Green, J., Pollard, J., Jr. & Tugendreich, S. Causal analysis approaches in Ingenuity Pathway Analysis. *Bioinformatics* **30**, 523-530 (2014).

46. Tarling, E.J. & Edwards, P.A. Dancing with the sterols: critical roles for ABCG1, ABCA1, miRNAs, and nuclear and cell surface receptors in controlling cellular sterol homeostasis. *Biochim Biophys Acta* **1821**, 386-395 (2012).

47. Zhao, C. & Dahlman-Wright, K. Liver X receptor in cholesterol metabolism. *J Endocrinol* **204**, 233-240 (2010).

48. Willy, P.J. *et al.* LXR, a nuclear receptor that defines a distinct retinoid response pathway. *Genes Dev* **9**, 1033-1045 (1995).

49. Shinar, D.M. *et al.* NER, a new member of the gene family encoding the human steroid hormone nuclear receptor. *Gene* **147**, 273-276 (1994).

50. Mottis, A., Mouchiroud, L. & Auwerx, J. Emerging roles of the corepressors NCoR1 and SMRT in homeostasis. *Genes Dev* **27**, 819-835 (2013).

51. Li, P. *et al.* NCoR repression of LXRs restricts macrophage biosynthesis of insulin-sensitizing omega 3 fatty acids. *Cell* **155**, 200-214 (2013).

52. Hu, X., Li, S., Wu, J., Xia, C. & Lala, D.S. Liver X receptors interact with corepressors to regulate gene expression. *Mol Endocrinol* **17**, 1019-1026 (2003).

53. Collins, J.L. *et al.* Identification of a nonsteroidal liver X receptor agonist through parallel array synthesis of tertiary amines. *J Med Chem* **45**, 1963-1966 (2002).

54. Michaels, A.J., Campbell, C., Bou-Puerto, R. & Rudensky, A.Y. Nuclear receptor LXRβ controls fitness and functionality of activated T cells. *J Exp Med* **218** (2021).

55. Michaels, A.J., Campbell, C., Bou-Puerto, R. & Rudensky, A.Y. Nuclear receptor LXRbeta controls fitness and functionality of activated T cells. *J Exp Med* **218** (2021).

56. Saravia, J. *et al.* Homeostasis and transitional activation of regulatory T cells require c-Myc. *Sci Adv* **6**, eaaw6443 (2020).

57. Angelin, A. *et al.* Foxp3 Reprograms T Cell Metabolism to Function in Low-Glucose, High-Lactate Environments. *Cell Metab* **25**, 1282-1293.e1287 (2017).

58. Zhuang, Q. *et al.* NCoR/SMRT co-repressors cooperate with c-MYC to create an epigenetic barrier to somatic cell reprogramming. *Nat Cell Biol* **20**, 400-412 (2018).

59. Mottet, C., Uhlig, H.H. & Powrie, F. Cutting edge: cure of colitis by CD4+CD25+ regulatory T cells. *J Immunol* **170**, 3939-3943 (2003).

60. Bensinger, S.J. *et al.* LXR signaling couples sterol metabolism to proliferation in the acquired immune response. *Cell* **134**, 97-111 (2008).

61. Andersen, L. *et al.* The Transcription Factor MAZR/PATZ1 Regulates the Development of FOXP3(+) Regulatory T Cells. *Cell Rep* **29**, 4447-4459 e4446 (2019).

62. Moolenbeek, C. & Ruitenberg, E.J. The "Swiss roll": a simple technique for histological studies of the rodent intestine. *Lab Anim* **15**, 57-59 (1981).

63. Hassan, H. *et al.* Cd8 enhancer E8I and Runx factors regulate CD8α expression in activated CD8+ T cells. *Proc Natl Acad Sci U S A* **108**, 18330-18335 (2011).

64. Seki, A. & Rutz, S. Optimized RNP transfection for highly efficient CRISPR/Cas9-mediated gene knockout in primary T cells. *J Exp Med* **215**, 985-997 (2018).

65. Gerner, M.C. *et al.* The TGF-b/SOX4 axis and ROS-driven autophagy co-mediate CD39 expression in regulatory T-cells. *Faseb j* **34**, 8367-8384 (2020).

Figures and Figure legends:

Figure 1

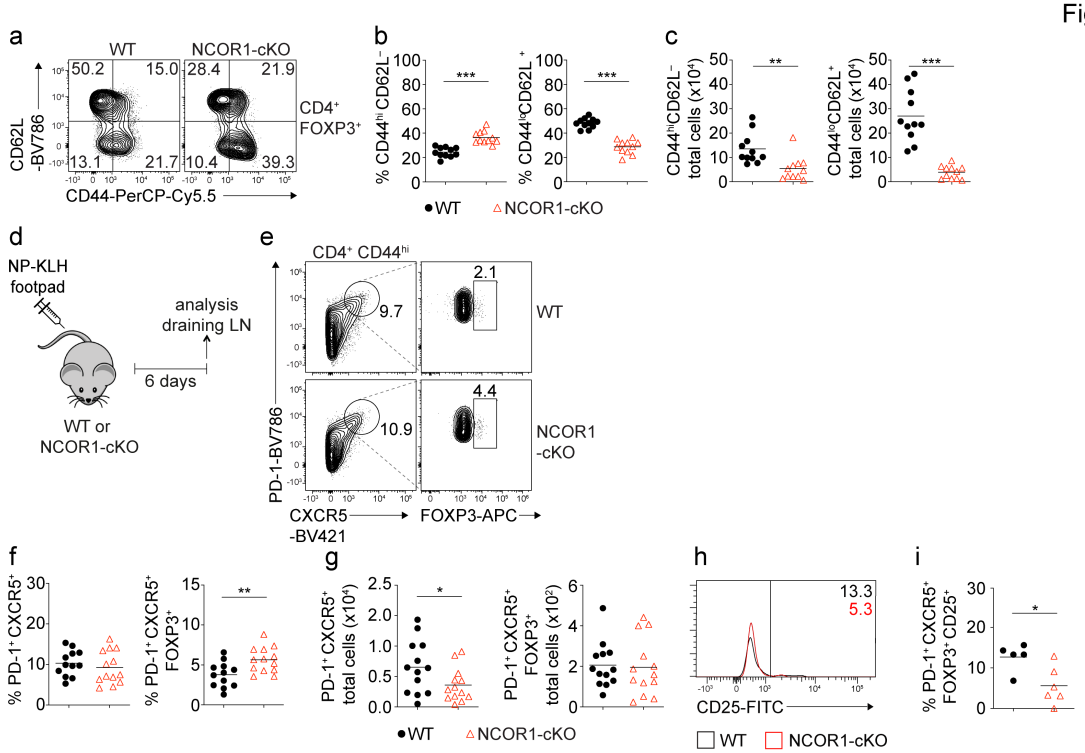

Figure 1. Loss of NCOR1 leads to a relative increase in CD44^{hi}CD62L^{-} effector Treg cells.

(a) Flow cytometric analysis of splenocytes isolated from WT and NCOR1-cKO mice showing CD44 and CD62L expression in CD4^{+}FOXP3^{+} cells at steady-state. **(b)** Diagram showing percentage of CD44^{hi}CD62L^{-} and CD44^{lo}CD62^{+} cells of all mice analyzed as described in (a). **(c)** Total cell numbers of CD44^{hi}CD62L^{-} and CD44^{lo}CD62^{+} cells of all mice analyzed described in (a). **(d)** Experimental immunization strategy: mice were injected s.c. with NP-KLH and draining LNs analyzed six days later. **(e)** Flow cytometric analysis of cells isolated from draining LN of NP-KLH-immunized WT and NCOR1-cKO mice showing the expression of PD-1, CXCR5 and FOXP3 on CD4^{+}CD44^{hi} cells. **(f)** Diagram showing percentage of Tfh cells (CD4^{+}CD44^{hi}PD1^{+}CXCR5^{+}) and Tfr cells (CD4^{+}CD44^{hi}PD1^{+}CXCR5^{+}FOXP3^{+}) of all mice analysed shown in (d,e). **(g)** Total cell numbers of Tfh cells (CD4^{+}CD44^{hi}PD1^{+}CXCR5^{+}) and Tfr cells (CD4^{+}CD44^{hi}PD1^{+}CXCR5^{+}FOXP3^{+}) of all mice analyzed shown in (d,e). **(h)** Flow cytometric analysis of cells isolated from draining LN of NP-KLH-immunized WT and NCOR1-

cKO mice showing the expression CD25 in $CD4^{+}CD44^{hi}PD1^{+}CXCR5^{+}FOXP3^{+}$ Tfr cells. **(i)** Percentage of CD25 expressing $CD4^{+}CD44^{hi}PD1^{+}CXCR5^{+}FOXP3^{+}$ Tfr cells of all mice analyzed shown in (d,e and h) **(a,e)** Numbers indicate the percentages of cells in the respective quadrants or gates. **(a-c)** Cells were pre-gated on CD4 and FOXP3. **(b,c,f,g,i)** Each symbol indicates one mouse. Horizontal bars indicate the mean. *$P < 0.05$, **$P < 0.01$, and ***$P < 0.001$; Unpaired 2-tailed Student's t test. Data are representative **(a,e,h)** or show the summary **(b,c,f,g,i)** of at least 11 **(b,c)**, 12 **(f,g**) or 5 **(i)** mice that were analyzed in at least 2 independent experiments.

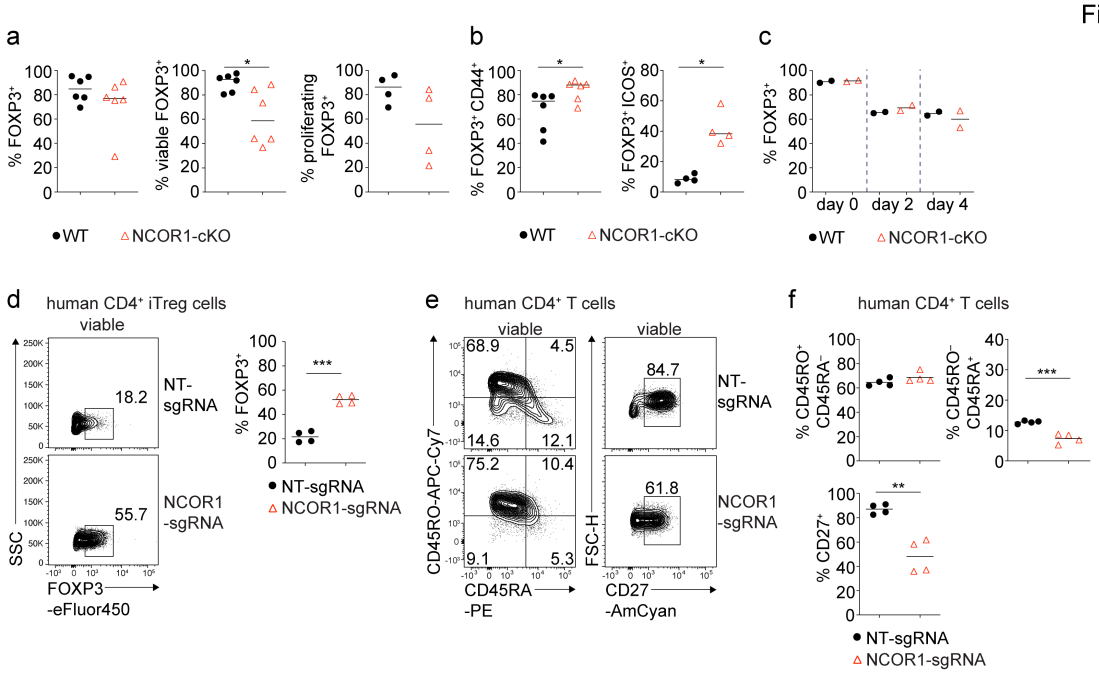

Figure 2. NCOR1 controls effector features in murine and human iTreg cells.

(a,b) Naïve WT and NCOR1-cKO CD4$^+$ T cells differentiated for 3 days in the presence of TGFβ and IL2. **(a)** **S**ummaries of the percentages of WT and NCOR1-cKO FOXP3$^+$, of viable FOXP3$^+$ and of proliferating FOXP3$^+$ iTreg cells at day 3. **(b)** **S**ummaries of the percentages of CD44^{hi} FOXP3$^+$ and ICOS$^+$ FOXP3$^+$ cells. **(c)** Maintenance of FOXP3 expression in iTreg cells differentiated from WT and NCOR1-cKO mice over the course of 3 days upon restimulation with anti-CD3/anti-CD28 in the absence of TGFβ. **(d)** Flow cytometric analysis showing FOXP3 expression in human CD4$^+$ T cells cultured under iTreg conditions after CRISPR-Cas9 mediated deletion of NCOR1 (NCOR1-sgRNA) or in non-targeting control samples (NT-sgRNA). Diagram at the right shows the summary of all experiments. **(e)** Flow cytometric analysis showing CD45RA, CD45RO and CD27 expression in human iTreg cells after CRISPR-Cas9 mediated deletion described in (d). **(f)** Summaries of the experiments described in (e). **(d,e)** Cells were pre-gated on total viable cell population. **(d,f)** Each symbol indicates one sample. Horizontal bars indicate the mean. *P < 0.05, **P < 0.01, and ***P < 0.001; unpaired 2-tailed Student's t test (**d,f**). Data are representative **(d,e)** or show the summary **(d,f)** of samples from 4 individual healthy donors which were analyzed in one experiment. **(a,b,c)** Each symbol indicates one mouse. Horizontal bars indicate the mean. *P

< 0.05, **P < 0.01, and ***P < 0.001. **(a,b,c)** Unpaired 2-tailed Student's t test. Data show a summary **(a,b,c)** of at least 2 mice that were analyzed in at least one experiment.

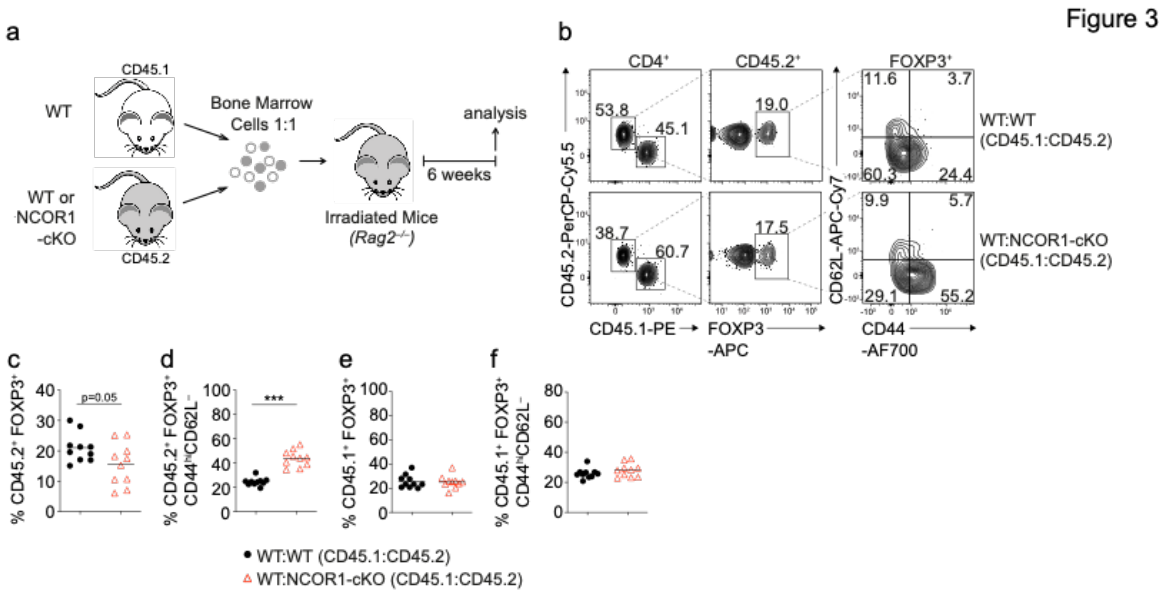

Figure 3. NCOR1 controls CD44^{hi}CD62L^{-} effector Treg cell differentiation in a Treg cell-intrinsic manner.

(a) Experimental strategy for generating bone marrow chimeric mice. **(b)** Flow cytometric analysis showing the distribution of CD45.1^{+} and CD45.2^{+} cells as well as the expression of FOXP3, CD44 and CD62L in recipient mice injected with either WT:WT or WT:NCOR1-cKO BM mixtures. **(c-f)** Summary of all experiments as described in (b) showing the percentages of FOXP3^{+} cells **(c,e)** and CD44^{hi}CD62L^{-} and CD44^{lo}CD62L^{+} expressing cells **(d,f)** within the **(c,d)** CD45.2^{+} population and the **(e,f)** CD45.1^{+} population isolated from the spleen of recipient *Rag2*$^{-/-}$ mice injected with either WT:WT or WT:NCOR1-cKO BM cell mixtures. **(b)** Numbers indicate the percentages of cells in the respective quadrants or gates. **(c-f)** Cells were pre-gated on CD4. Each symbol indicates one mouse. Horizontal bars indicate the mean. *P < 0.05, **P < 0.01, and ***P < 0.001; unpaired 2-tailed Student's t test. Data are representative **(b)** or show a summary **(c-f)** of 10 mice that were analyzed in 2 independent experiments.

Figure 4

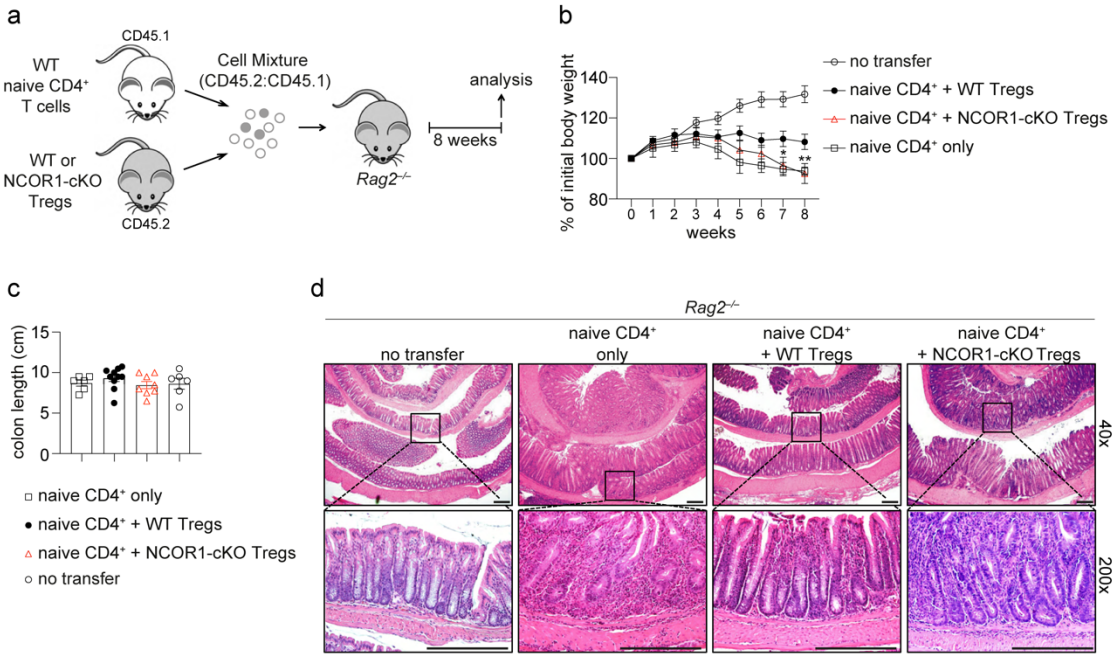

Figure 4. NCOR1 is essential for Treg-mediated protection in adoptive CD4⁺ T cell transfer colitis.

(a) Experimental protocol for adoptive transfer colitis. Control groups received naïve CD4⁺ T cells only (as indicated) or no cells at all (not shown). **(b)** Weight scores in percentages of initial body weight during the course of colitis in *Rag2*$^{-/-}$ recipient mice are shown. Data show the summary of at least 8 mice (except control groups with 6 mice) of 3 independent experiments. *P < 0.05, **P < 0.01, and ***P < 0.001 (2-way ANOVA analysis followed by Tukey's multiple-comparisons test). For simplicity, significant differences are shown only between WT and NCOR1-cKO Treg cells. Of note, non-injected control mice gained significantly more weight compared to all groups starting from week 5. **(c)** Summary showing lengths of colons isolated from *Rag2*$^{-/-}$ recipient mice. **(d)** Colon swiss rolls were processed for H&E staining. The pictures in the bottom represent a 5x magnification of the black rectangle framed section in the top pictures. Magnification: 40x and 200x. Scale bar = 100µm. One representative picture is shown per condition.

Figure 5

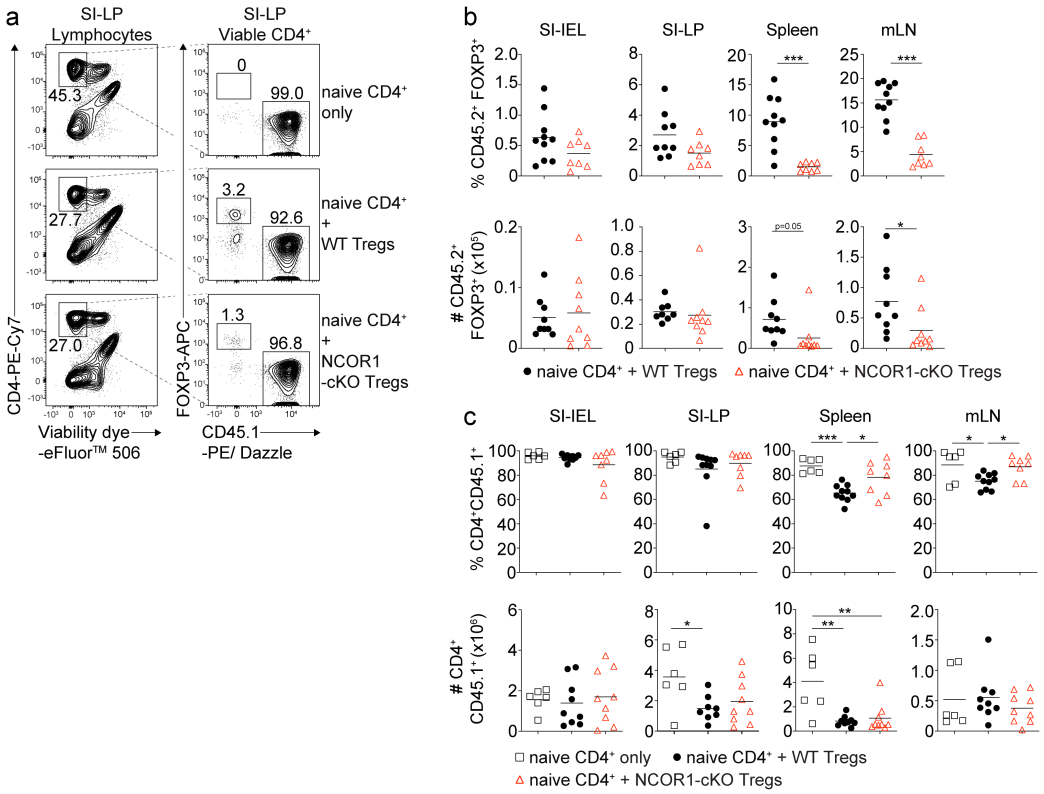

Figure 5. Similar numbers of WT and NCOR1-deficient Treg cells in SI-IEL and SI-LP after adoptive transfer.

(a) Flow cytometric analysis of SI-LP cells isolated from WT and NCOR1-cKO mice showing percentage of viable $CD4^+$, $CD45.2^+FOXP3^-$ and $CD45.1^-FOXP3^+$ cells. **(b)** Summaries of the percentages (upper panel) and numbers (lower panel) of $CD45.2^+FOXP3^+$ cells isolated from SI-IEL, SI-LP, spleen and mLNs of recipient *Rag2*$^{-/-}$ mice injected with WT $CD45.1^+CD4^+$ T cells together with either WT or NCOR1-cKO Treg cells. **(c)** Summary of the percentages (upper panel) and numbers (lower panel) of $CD4^+CD45.1^+$ cells isolated from SI-IEL, SI-LP, spleen and mLNs of *Rag2*$^{-/-}$ mice injected with either WT Treg cells, NCOR1-cKO Treg cells or injected with naïve $CD4^+$ T cells only. **(a)** Numbers indicate the percentages of cells in the respective gate. **(b,c)** Each symbol indicates one mouse. Horizontal bars indicate the mean. *P < 0.05, **P < 0.01, and ***P < 0.001. **(b)** Unpaired 2-tailed Student's t test or **(c)** ordinary 1-way ANOVA analysis followed by Tukey's multiple-comparisons test. Data are representative **(a)** or show a summary **(b,c)** of at least 8 mice (except control groups with 6 mice) that were analyzed in 3 independent experiments.

Figure 6. Naïve NCOR1-cKO Treg cells upregulate an effector gene signature.

(a) Contour plots show the gating strategy for the isolation of cells for RNA-sequencing. Cells from spleen and LNs of WT.DEREG and NCOR1-cKO.DEREG mice were isolated and $FOXP3^{+}CD44^{hi}CD62L^{-}$ and $FOXP3^{+}CD44^{lo}CD62L^{+}$ cells were sorted and sequenced using the Illumina HiSeq 3000 platform. **(b)** Volcano plots depict a comparison of global gene expression profiles between naïve ($CD44^{lo}CD62L^{+}$) WT and NCOR1-cKO Treg cells (left plot) and effector ($CD44^{hi}CD62L^{-}$) WT and NCOR1-cKO Treg cells (right plot). On the x-axis log2-fold change is plotted, while the y-axis indicates adjusted p-values (-log10). 1027 genes were downregulated and 540 genes were upregulated in naïve NCOR1-cKO Treg cells. 275 and 299 genes were down- and upregulated, respectively, in effector NCOR1-cKO Treg cells. In addition to *Ncor1* and *Myc*, the top 5 genes leading to enrichment of cholesterol homeostasis (*) and of Myc targets v2 hallmark gene signatures are shown. **(c)** Diagram showing the top hits of enriched hallmark gene signatures in WT (NES <0) and NCOR1-cKO (NES >0) naïve (top) and effector (bottom) Treg cells. The x axis indicates the Z score. **(d)** Gene set enrichment analysis (GSEA) plots of an “effector Treg gene set” (containing a list of 100 genes) in naïve NCOR1-cKO Treg cells compared to naïve WT Treg cells. **(e)** Gene set enrichment analysis (GSEA) plots of a “naïve Treg gene set” (containing a list of 100 genes) in effector NCOR1-cKO Treg cells compared to effector WT Treg cells. **(d,e)** Barcodes indicate the location of the members of the gene set in the ranked list of all genes. NES, normalized enrichment score in WT Treg cells compared to NCOR1-cKO Treg cells. The lists of the “naïve Treg gene set” and the “effector Treg gene set” are provided in Supplementary Table 7.

Figure 7

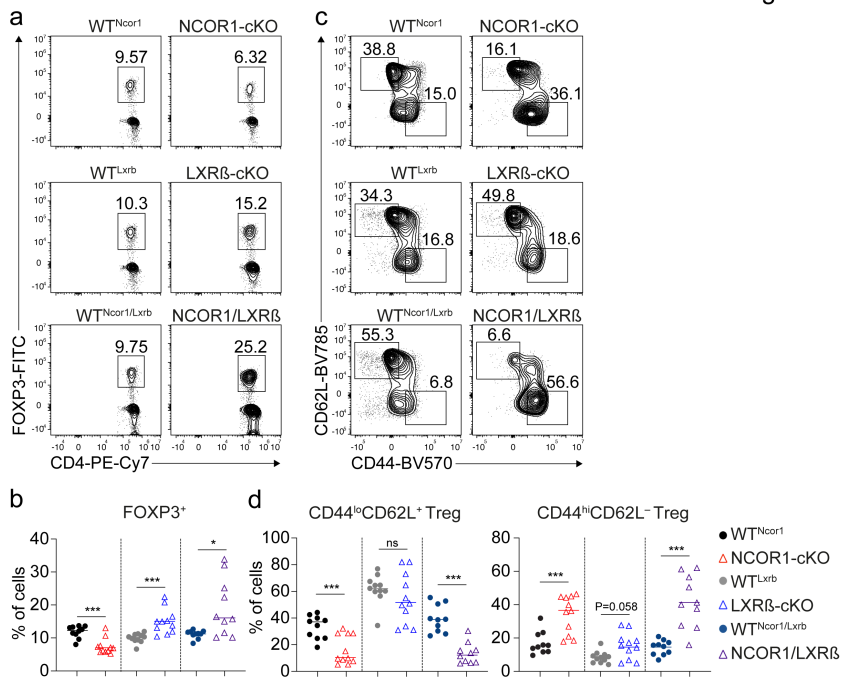

Figure 7. NCOR1 controls naïve and effector Treg cells in an LXRß-independent manner.

(a) Contour plots show FOXP3 and CD4 expression in splenocytes of mice of the indicated genotype. (**b**) Percentages of FOXP3$^+$ CD4$^+$ T cells of all mice analyzed as described in (a). **(c)** Flow cytometric analysis of splenocytes isolated from mice of the indicated genotype showing CD44 and CD62L expression in CD4$^+$FOXP3$^+$ T cells at steady-state. **(d)** Percentage of CD44^{hi}CD62L$^-$ and CD44^{lo}CD62$^+$ cells of all mice analyzed as described in (c). (**a**,**c**) Numbers next to the regions indicate the frequency of cells. **(b,d)** Each symbol indicates one mouse. Horizontal bars indicate the mean. *P < 0.05, **P < 0.01, and ***P < 0.001. **(b,d)** Unpaired 2-tailed Student's t tests comparing respective WT and knockout samples. Data are representative (**a**,**c**) or show the summary (**b**,**d**) of at least 10 mice that were analyzed in at least 8 independent experiments.

Supplementary Figures:

Nuclear receptor corepressor 1 controls regulatory T cell subset differentiation and effector function

Authors: Valentina Stolz[1,#], Rafael de Freitas e Silva[1,#], Ramona Rica[1], Ci Zhu[1], Teresa Preglej[1], Patricia Hamminger[1], Daniela Hainberger[1], Marlis Alteneder[1], Lena Müller[1], Monika Waldherr[1], Darina Waltenberger[1], Anastasiya Hladik[2], Benedikt Agerer[3], Michael Schuster[3], Tobias Frey[4], Thomas Krausgruber[3,7], Sylvia Knapp[2], Clarissa Campbell[3], Klaus Schmetterer[4], Michael Trauner[5], Andreas Bergthaler[3,6], Christoph Bock[3,7], Nicole Boucheron[1], Wilfried Ellmeier[1,*]

[1]Medical University of Vienna, Center for Pathophysiology, Infectiology and Immunology, Institute of Immunology, Vienna, Austria.
[2]Medical University of Vienna, Vienna, Department of Medicine I, Laboratory of Infection Biology, Vienna, Austria.
[3]CeMM Research Centre for Molecular Medicine of the Austrian Academy of Sciences, Vienna, Austria.
[4]Medical University of Vienna, Department of Laboratory Medicine, Vienna, Austria.
[5]Medical University of Vienna, Department of Internal Medicine III, Division of Gastroenterology and Hepatology, Hans Popper Laboratory of Molecular Hepatology, Vienna, Austria.
[6]Medical University of Vienna, Vienna, Center for Pathophysiology, Infectiology and Immunology, Institute for Hygiene and Applied Immunology, Austria.
[7]Medical University of Vienna, Center for Medical Statistics, Informatics, and Intelligent Systems, Institute of Artificial Intelligence, Vienna, Austria.

equal first-authorship
*Corresponding author: Wilfried Ellmeier; wilfried.ellmeier@meduniwien.ac.at

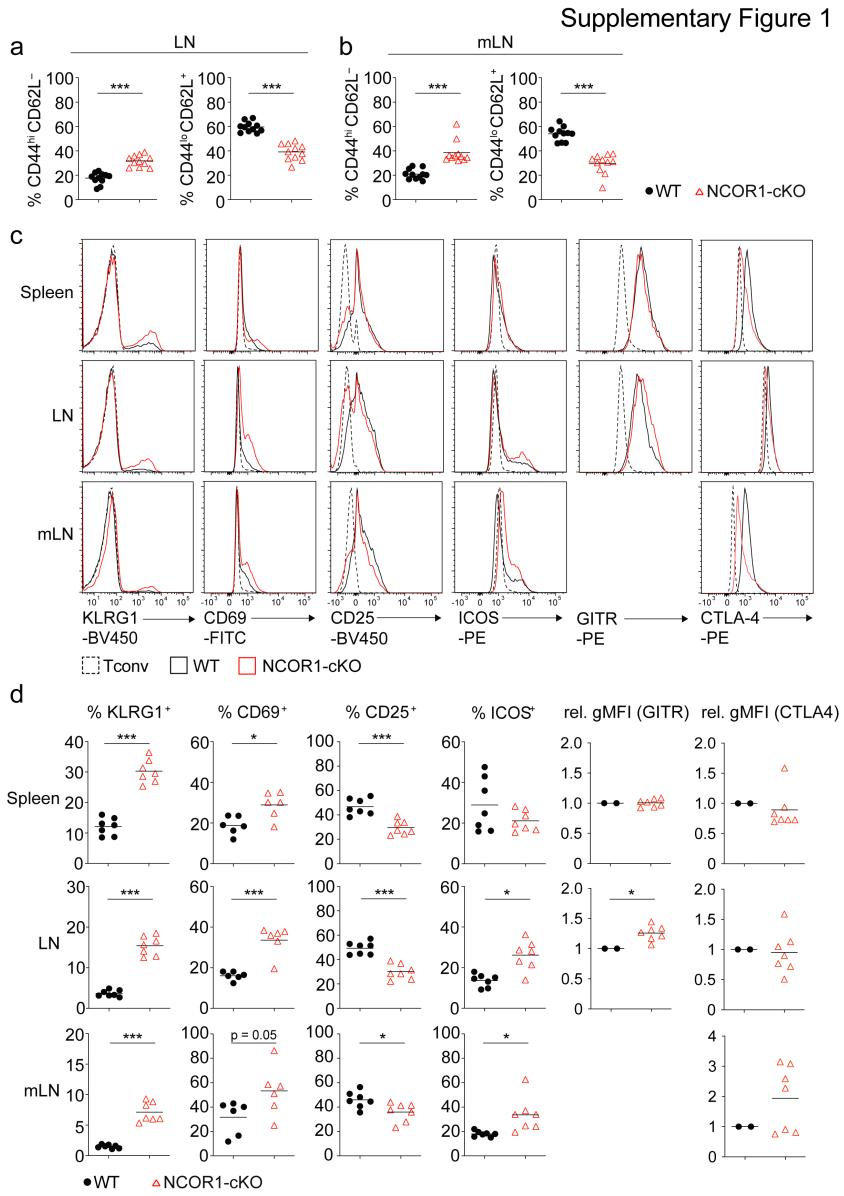

Supplementary Figure 1. Effector markers are upregulated in NCOR1-deficient Treg cells.

(a) Diagrams showing a summary of the percentage of CD44^{hi}CD62L^{-} and CD44^{lo}CD62L^{+} cells isolated from LNs of WT and NCOR1-cKO mice. **(b)** Diagrams showing a summary of the percentage of CD44^{hi}CD62L^{-} and CD44^{lo}CD62L^{+} cells isolated from mLNs of WT and NCOR1-cKO mice. **(a,b)** Cells were pregated on CD4. **(c)** Histograms displaying expression of CD25, CD103, KLRG1, ICOS, CD69, GITR and CTLA4 in WT and NCOR1-cKO Treg cells isolated from spleen, LNs and mLNs. **(d)** Diagrams showing the summary of all analysis performed as shown in (c). For the calculation of GITR and CTLA4 relative gMFI levels, the

average expression levels in WT cells (n=4 in experiment 1 and n=3 in experiment 2) were set as 1 and relative gMFI on individual NCOR1-cKO Treg samples (n=4, and n=3) was calculated. **(a,b,d)** Each symbol indicates one mouse. Horizontal bars indicate the mean. *P < 0.05, **P < 0.01, and ***P < 0.001; unpaired 2-tailed Student's t test. Data are representative **(c)** or show a summary **(a,b,d)** of at least 7 mice analyzed in at least 2 independent experiments.

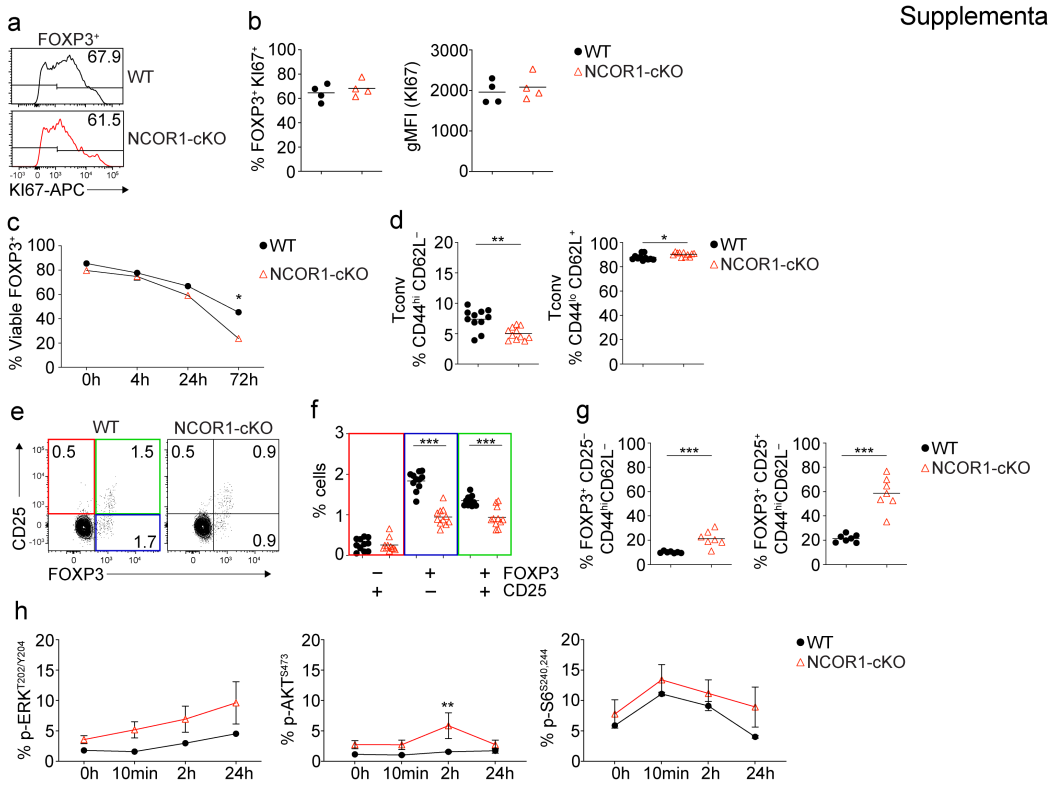

Supplementary Figure 2. Characterization of FOXP3⁺ Treg cells isolated from NCOR1-cKO mice.

(a) Flow cytometric analysis of *ex vivo* splenocytes of WT and NCOR1-cKO mice showing expression of Ki67 in CD4⁺ FOXP3⁺ cells under steady state. **(b)** Summary showing percentage and expression (gMFI) of KI67 in CD4⁺FOXP3⁺ cells of all mice analyzed as described in (g). **(c)** Summary showing the percentage of viable FOXP3⁺ splenocytes cultured in the presence of anti-CD3/anti-CD28 over the course of 3 days. **(d)** Diagrams showing summary of the percentages of and CD44^{hi}CD62L⁻ (left) and CD44^{lo}CD62L⁺ (right) CD4⁺ T cells (FOXP3⁻) cells isolated from the spleen of WT and NCOR1-cKO mice. **(e)** Flow cytometry analysis showing FOXP3 and CD25 expression of thymocytes isolated from WT and NCOR1-cKO mice. **(f)** Diagram showing percentage of FOXP3⁻CD25⁺, FOXP3⁺CD25⁻ and FOXP3⁺CD25⁺ thymocytes of all mice analyzed as described in (b). **(g)** Diagrams showing the summary of thymic FOXP3⁺CD25⁻CD44^{hi}CD62L⁻ and FOXP3⁺CD25⁺CD44^{hi}CD62L⁻ cells isolated from WT and NCOR1-cKO mice**.** Thymocytes were pre-gated on CD4⁺. **(h)** Summary showing the percentage of phospho-ERK$^{T202/Y204}$, phospho-AKT^{S473} and phospho-S6$^{S240/244}$

expression in FOXP3$^+$ splenocytes cultured in the presence of anti-CD3/anti-CD28 over the course of 24 hours. **(b)** Numbers indicate the percentages of cells positive for KI67. **(e)** Numbers indicate the percentages of cells in the respective quadrants. **(b,d,f,g,h)** Each symbol indicates one mouse. Horizontal bars indicate the mean. *P < 0.05, **P < 0.01, and ***P < 0.001. **(b,d,f,g,h)** Unpaired 2-tailed Student's t test, **(c,h)** 2-way ANOVA analysis followed by Tukey's multiple-comparisons test). Data are representative **(a,e)** or show a summary **(c,d,f,g,h)** of at least 2 independent samples **(c,d,h)** or at least seven mice **(f,g)** that were analyzed in at least one **(c,d,h)** or 3 **(f,g)** independent experiments.

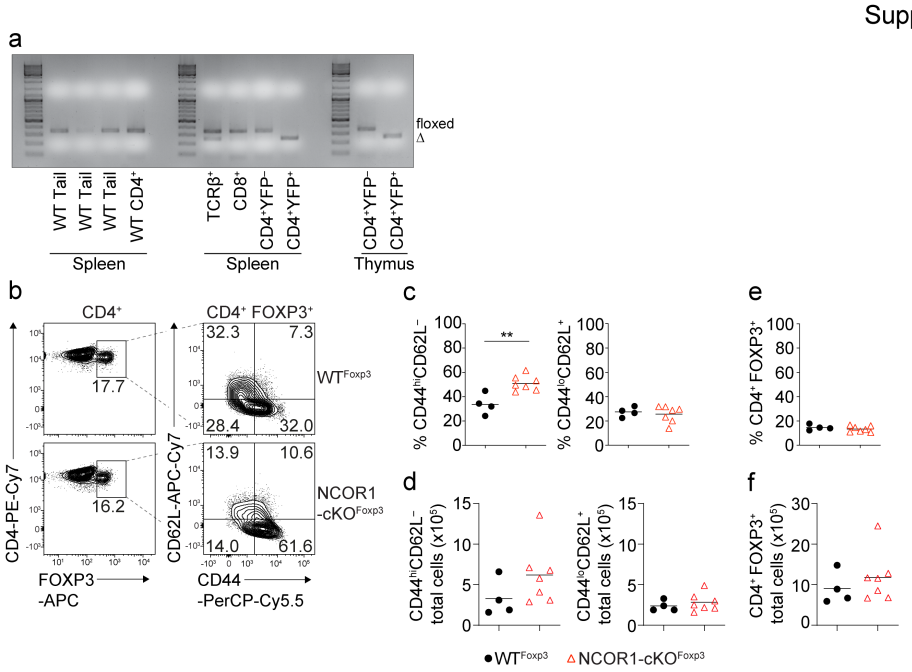

Supplementary Figure 3. Treg cell-specific deletion of NCOR1 results in enhanced CD44^{hi}CD62L^{-} effector Treg subsets.

(a) Representative agarose gel picture showing *Ncor1* deletion PCR in WT tail samples and FACS-sorted WT CD4^{+} splenocytes (left panel), TCRß$^{+}$, CD8^{+}, CD4^{+}YFP^{-} and CD4^{+}YFP^{+} cells isolated from the spleen of NCOR1-cKO^{Foxp3} mice (middle panel) and CD4^{+}YFP^{-} and CD4^{+}YFP^{+} cells isolated from the thymus (right panel) of NCOR1-cKO^{Foxp3} mice. Two mice were pooled for sorting. Size floxed band: 346bp. Size Δ band: 246bp. **(b)** Flow cytometric analysis of FOXP3, CD44 and CD62L expression on splenic CD4^{+} T cells isolated from WT^{Foxp3} and NCOR1-cKO^{Foxp3} mice. **(c)** A summary of the percentage of splenic CD44^{hi}CD62L^{-} and CD44^{lo}CD62L^{+} cells isolated from WT^{Foxp3} and NCOR1-cKO^{Foxp3} mice. **(d)** The summary of total cell numbers of splenic CD44^{hi}CD62L^{-} and CD44^{lo}CD62L^{+} cells isolated from WT^{Foxp3} and NCOR1-cKO^{Foxp3} mice. **(e)** Summary showing of the percentage of splenic CD4^{+}FOXP3^{+} cells isolated from WT^{Foxp3} and NCOR1-cKO^{Foxp3} mice. **(f)** The summary of total cell numbers of splenic CD4^{+}FOXP3^{+} cells isolated from WT^{Foxp3} and NCOR1-cKO^{Foxp3} mice.

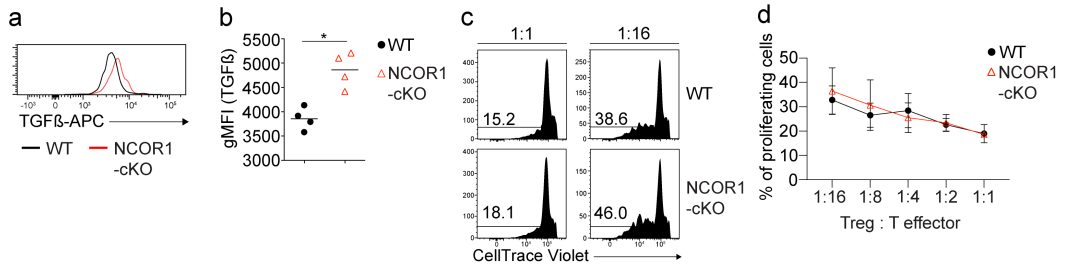

Supplementary Figure 4. *In vitro* characterization of NCOR1-cKO and WT Treg cells.

(a) Flow cytometric analysis of splenocytes isolated from WT and NCOR1-cKO mice showing expression of TGFβ in $CD4^+FOXP3^+$ Treg cells after stimulation with PMA/ ionomycin for 4 hours. **(b)** Summary showing TGFβ expression (gMFI) in $FOXP3^+$ Treg cells of all mice analyzed described in (a). **(c)** Histograms showing the proliferation of naïve $CD4^+$ T cells co-cultured in the presence of either WT or NCOR1-cKO Treg cells at different ratios. **(d)** Summary showing the results of the experiment described in (c). **(c)** Numbers indicate the percentages of cells in the respective gates. **(b,d)** Each symbol indicates one mouse or sample. **(b)** Horizontal bars indicate the mean. *P < 0.05, **P < 0.01, and ***P < 0.001. Unpaired 2-tailed Student's t test. Data are representative **(a,c)** or show a summary **(b,d)** of 4 (**a**) or at least 2 independent samples (**c**) or (**d**) that were analyzed in one experiment (**a**) or in 2 (**c**) independent experiments.

Supplementary Figure 5

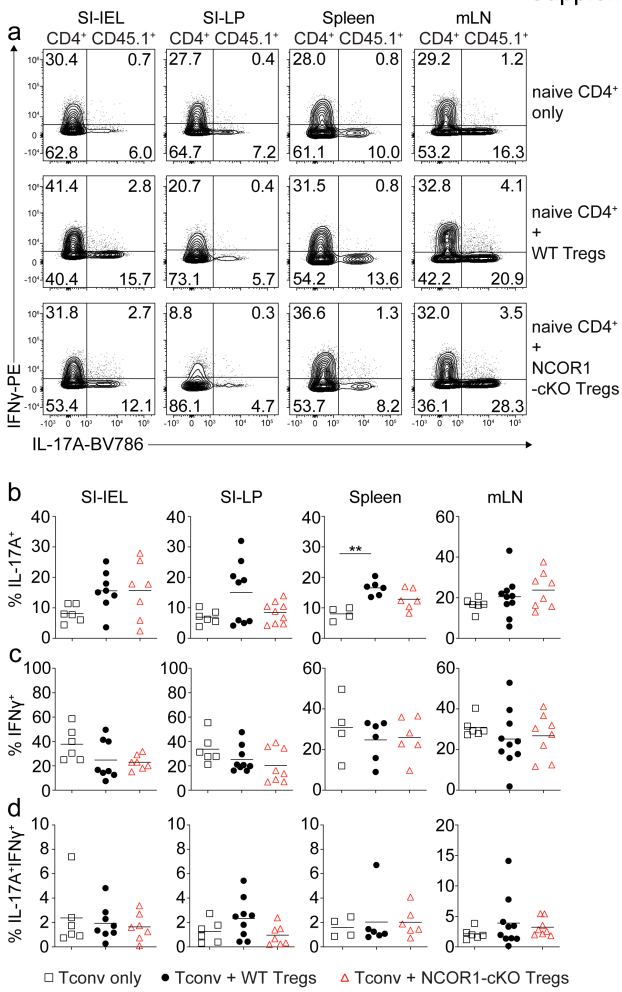

Supplementary Figure 5. Similar percentages of IFNγ and IL17A expression in CD4⁺ T cells co-transferred with either WT of NCOR1-cKO Treg cells.

(a) Flow cytometric analysis showing IFNγ and IL17A expression in CD45.1⁺ CD4⁺ T cells isolated from SI-IEL, SI-LP, spleen and mLNs. **(b)** Summary of all experiments described in (a). **(a,b)** Cells were pre-gated on CD4. **(a)** Numbers indicate the percentages of cells in the respective quadrants. **(b)** Each symbol indicates one mouse. Horizontal bars indicate the mean. *P < 0.05, **P < 0.01, and ***P < 0.001; 1-way ANOVA analysis followed by Tukey's multiple-comparisons test. Data are representative **(a)** or show the summary **(b)** of at least 6 mice (except CD4⁺ T cells only controls with at least 4 mice) that were analyzed in 3 independent experiments.

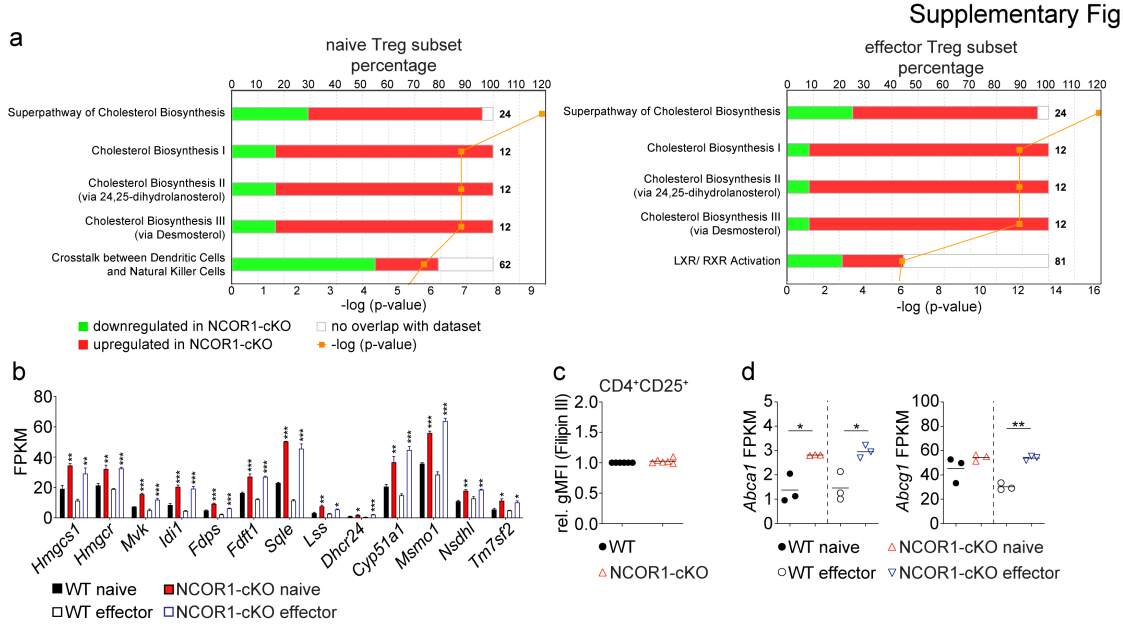

Supplementary Figure 6. Loss of NCOR1 leads to an upregulation of cholesterol pathways.

(a) Diagram showing top 5 pathways which are up- or downregulated in naïve (left) and effector (right) NCOR1-cKO Treg cells, as revealed by Ingenuity Pathway Analysis (QIAGEN Inc.). The lower x-axis indicates the p-value. The upper x-axis indicates the percentage of genes dysregulated in this particular pathway. The number next to the bar indicates the number of genes in this pathway. A list of all pathways identified by Ingenuity Pathway Analysis is provided in Supplementary Table 5 and 6. **(b)** Summary showing the expression levels (values showing as fragments per kilobase of transcript per million mapped reads; FPKM) of genes controlling cholesterol biosynthesis in naïve and effector WT and NCOR1-cKO Treg cells as determined by RNA-seq. **(c)** Summary showing Filipin III staining (rel. gMFI) in WT and NCOR1-cKO Treg cells pre-gated on cells expressing CD4 and CD25. For gMFI calculation, WT levels were set as 1 and relative gMFI of Filipin III is shown. **(d)** Summary showing FPKM values of *Abca1* and *Abcg1* in naïve and effector WT and NCOR1-cKO WT Treg cells as determined by RNA-seq. **(b)** Each bar represents 3 mice per group. **(c,d)** Each symbol indicates one mouse (c,d) or one sample (e). **(b-d)** Horizontal bars indicate the mean. *P < 0.05, **P < 0.01, and ***P < 0.001 **(b,d)** ordinary 1-way ANOVA analysis followed by Tukey's multiple-comparisons test; for simplicity, significant differences are shown only

between WT and NCOR1-cKO Treg cells. **(c)** unpaired 2-tailed Student's t test. **(d)** Data show a summary of at least 6 mice that were analyzed in 2 independent experiments.

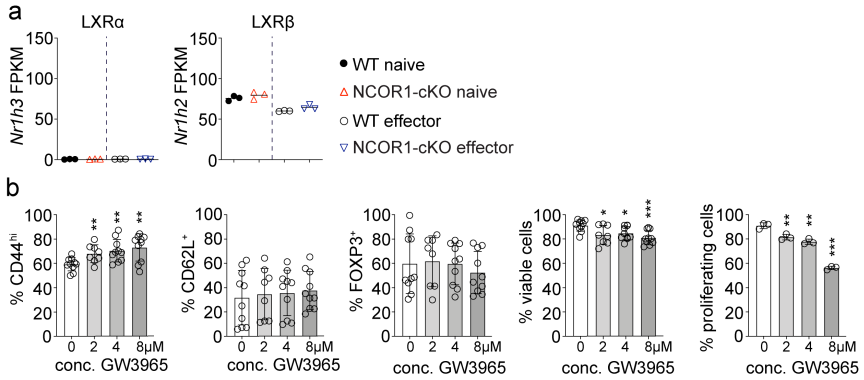

Supplementary Figure 7. LXRβ agonist-treatment of WT iTreg cells results in increased MYC expression.

(a) Summary showing the expression levels (values shown as fragments per kilobase of transcript per million mapped reads; FPKM) of *Nr1h3* (LXRα) and *Nr1h2* (LXRβ) in naïve and effector WT and NCOR1-cKO Treg cells as determined by RNA-seq. (**b**) Naïve WT $CD4^+$ T cells were cultured under iTreg cell-inducing conditions in the presence of the indicated amounts of GW3965 (or DMSO as control). The summary shows the percentage of $FOXP3^+CD44^{hi}$ cells, $FOXP3^+CD62L^-$ cells, $FOXP3^+$ cells and viable cells. The right diagram indicates the percentage of $FOXP3^+$ cells which underwent ≥ 1 cell division that have been treated with GW3965 or DMSO (as mock control). **(a,b)** Each symbol indicates one sample. Horizontal bars indicate the mean. *P < 0.05, **P < 0.01, and ***P < 0.001. **(a)** -way ANOVA analysis followed by Tukey's multiple-comparisons or (**b**) unpaired 2-tailed Student's t tests comparing respective GW3965- treated sample with mock (DMSO)-treated control. Data show the summary **(a,b)** of 3 (**a**) or at least 8 independent samples (**b**) that were analyzed in at least 3 independent experiments.

Supplementary Figure 8

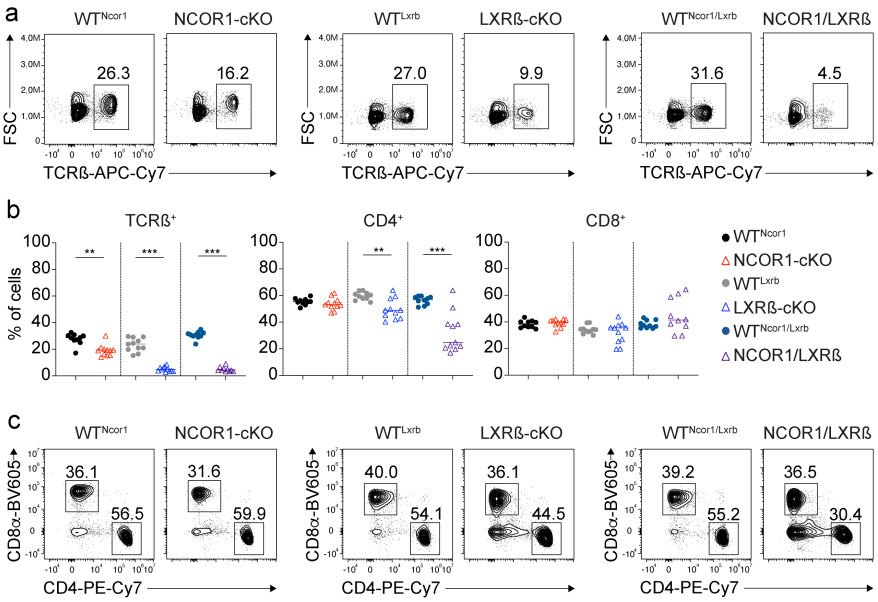

Supplementary Figure 8. Phenotypic characterization of NCOR1/LXRß-cDKO mice.

(**a**) Contour plots show TCRß expression on and cell size (forward-scatter; FSC) of splenocytes of mice of the indicated genotype. (**b**) Diagram indicates the frequency of TCRß$^+$ T cells as well as of CD4$^+$TCRß$^+$ and CD8$^+$TCRß$^+$ T cells of all mice analyzed described in (a) and (c). (**c**) Flow cytometric analysis of splenocytes isolated from mice of the indicated genotype showing CD4 and CD8 expression on TCRß$^+$ T cells at steady-state. (**a**,**c**) Numbers next to the regions indicate the percentage of cells. (**b**) Each symbol indicates one mouse. Horizontal bars indicate the mean. *P < 0.05, **P < 0.01, and ***P < 0.001. t-test and Wilcoxon-ranked column statistics. Data are representative (**a**,**c**) or show the summary (**b**) of at least 10 mice that were analyzed in at least 8 independent experiments.

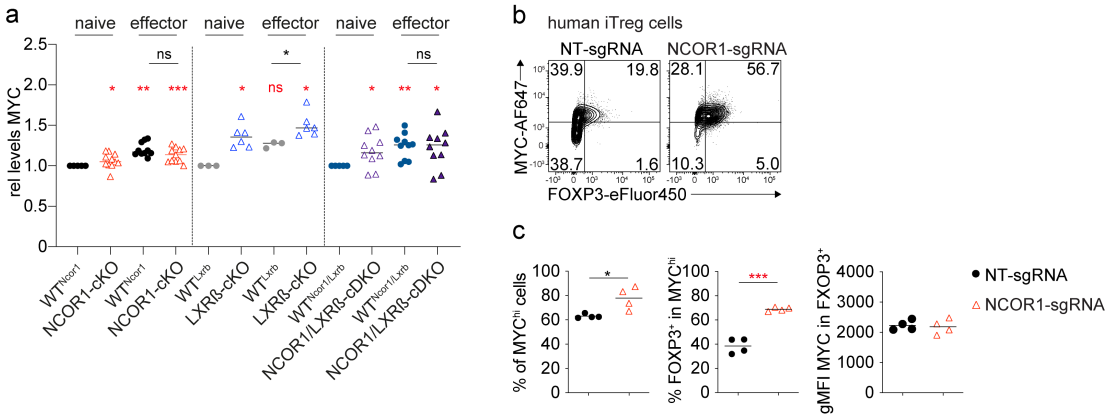

Supplementary Figure 9. NCOR1-deficient Treg cells exhibit increased expression of MYC.

(**a**) Diagram indicates MYC expression levels (geometric mean fluorescence intensity; gMFI) in naïve ($CD44^{lo}CD62^{+}$) and effector ($CD44^{hi}CD62L^{-}$) Treg cells of the indicated genotype. For gMFI calculations, MYC expression levels in naïve WT levels were set as 1 and relative gMFI of MYC is shown. (**b**) Flow cytometric analysis showing MYC and FOXP3 expression in human $CD4^{+}$ T cells cultured under iTreg conditions after CRISPR-Cas9 mediated deletion of NCOR1 (NCOR1-sgRNA) or in non-targeting control samples (NT-sgRNA). The same human $CD4^{+}$ T cell cultures as shown in Figure 2 were analyzed. (**c**) Diagrams show the summary of the experiments described in (b). The percentage of MYC-high (MYC^{hi}) cells (left), the frequency of $FOXP3^{+}$ cells with the MYC^{hi} population (middle) and gMFI of MYC within $FOXP3^{+}$ cells is shown (right). (**b**) Cells were pre-gated on the total viable cell population. (**a,c**) Each symbol indicates one mouse or sample. (**a,c**) Horizontal bars indicate the mean. *P < 0.05, **P < 0.01, and ***P < 0.001. (c) unpaired 2-tailed Student's t test; (**a**) Red fonts: t-test and Wilcoxon-ranked column statistics; black fonts: unpaired 2-tailed Student's t tests comparing MYC gMFI levels between the respective WT and knockout effector ($CD44^{hi}CD62L^{-}$) Treg cells. Data are representative (**b**) or show a summary of 4 individual healthy donors (**b,c**) or at least 10 mice (**a**) that were analyzed in one (**c**) or in at least 8 (**a**) independent experiments.

Supplementary Figure 10

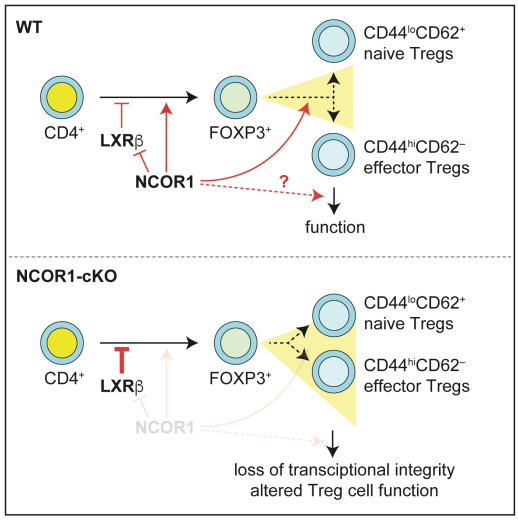

Supplementary Figure 10. NCOR1 positively regulates FOXP3$^+$ Treg cell differentiation and controls naïve and effector Treg cell subset integrity.

In the absence of NCOR1, Treg cell frequencies within the CD4$^+$ T cell population are decreased. In contrast, LXRß restrains Treg cell differentiation, since deletion of LXRß results in increased Treg cell frequencies among CD4$^+$ T cells. Deletion of LXRß on top of NCOR1 deletion reverts the NCOR1-cKO phenotype, indicating that NCOR1 controls Treg differentiation in an LXRß-dependent manner. NCOR1 might directly suppress LXRβ or counteracts LXRβ-controlled pathways, which are enhanced in the absence of NCOR1. The deletion of NCOR1 alters naïve and effector Treg cell subset composition and leads to a blurring of the transcriptional separation of naïve and effector Treg cell lineages. The deletion of LXRβ in the T cell lineage did not recapitulate the increase in CD44^{hi}CD62L$^-$ effector Treg cells in the spleen observed in NCOR1-cKO mice. The combined deletion of NCOR1 and LXRβ resulted in a strong increase in LXRβ-NCOR1 effector Treg cells and a corresponding severe reduction in naïve Treg cells, similar to the phenotype observed in NCOR1-cKO mice. This strongly suggests that NCOR1 controls the relative composition of naïve and effector Treg cell subsets in a LXRß-independent manner. See text for more details.

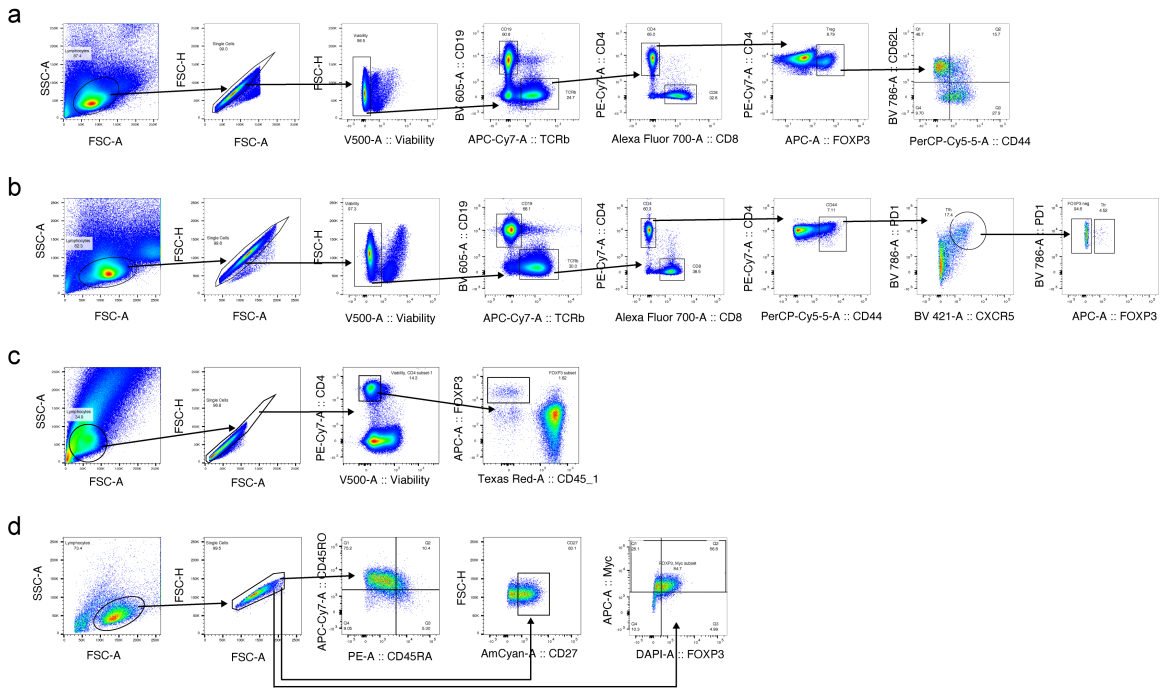

Supplementary Fig 11. Gating strategies for Flow Cytometric analysis.

(a) Gating strategy for identification of effector ($CD44^{hi}CD62L^{-}$) and naïve ($CD44^{lo}CD62L^{+}$) Treg cells: After exclusion of debris (FSC-A/ SSC-A), doublets (FSC-H/ FSC-W) and dead cells (using Viability Dye eFluor 506 or 780), cells were distinguished via their expression of CD19 (BV605) and TCRβ (BV711), CD4 (PE-Cy7) and CD8 (AF700) and FOXP3 (APC). Cells were further gated based on their expression of CD44 (PerCP-Cy5.5) and CD62L (APC-Cy7). **(b)** Gating strategies for identification of Tfh ($CXCR5^{+}PD1^{+}CD44^{hi}$) and Tfr ($CXCR5^{+}PD1^{+}CD44^{hi}FOXP3^{+}$) cells: Debris, doublets and dead cells were excluded as described in (a). Cells were distinguished via their expression of CD19 (BV605) and TCRβ (BV711), CD4 (PE-Cy7) and CD8 (AF700), CD44 (PerCP-Cy5.5), CXCR5 (BV421) and PD-1 (BV786) and FOXP3 (APC). **(c)** Gating strategy for MYC^{+} cells: effector and naïve Treg cells or total-Treg cells were gated as described in (a). Cells were further analysed via their expression of MYC (AF647) (gMFI). **(d)** Gating strategy for transfer colitis experiment: After exclusion of debris (FSC-A/ SSC-A) and doublets (FSC-H/ FSC-W) cells were distinguished via their expression of CD4 (PE-Cy7) and their viability using the Viability Dye eFluor 506. Cells were further gated based on their expression of CD45.1 (PE/ Dazzle) and FOXP3 (APC).

(d) Gating strategy for CRISPR-Cas9 mediated deletion experiments: After exclusion of debris (FSC-A/ SSC-A) and doublets (FSC-H/FSC-W) cells were distinguished via their expression of FOXP3 (eFluor 450) and MYC (AF647) or via their expression of the markers CD45RA (PE), CD45RO (APC-Cy7) and CD27 (AmCyan).